EXPERIMENTAL AND NUMERICAL ANALYSIS OF A SALT GRADIENT SOLAR POND

A THESIS SUBMITTED TO
THE BOARD OF CAMPUS GRADUATE PROGRAMS OF
MIDDLE EAST TECHNICAL UNIVERSITY
NORTHERN CYPRUS CAMPUS

BY

PELİN GÜVEN

IN PARTIAL FULFILLMENT OF THE REQUIREMENTS
FOR
THE DEGREE OF MASTER OF SCIENCE
IN
SUSTAINABLE ENVIRONMENT AND ENERGY SYSTEMS

SEPTEMBER 2018

Approval of the Board of Graduate Programs

_____

Prof. Dr. Gürkan Karakaş
Chairperson

I certify that this thesis satisfies all the requirements as a thesis for the degree of Master of Science.

_____

Asst. Prof. Dr. Ceren İnce Derogar
Program Coordinator

This is to certify that we have read this thesis and that in our opinion it is fully adequate, in scope and quality, as a thesis for the degree of Master of Science.

_____	_____
Asst. Prof. Dr. Mehdi A. Torkmahalleh Co-Supervisor	Asst. Prof. Dr. Onur Taylan Supervisor

Examining Committee Members

Asst. Prof. Dr. Onur Taylan _____
Mechanical Engineering Prog. METU NCC

Asst. Prof. Dr. Mehdi A. Torkmahalleh _____
Chemical Engineering Dept. Nazarbayev Uni.

Prof. Dr. Serkan Abbasoğlu _____
Energy Systems Engineering Prog. CIU

Assoc. Prof. Dr. Murat Fahrioğlu _____
Electrical & Electronics Engineering Prog. METU NCC

Asst. Prof. Dr. Bertuğ Akıntuğ _____
Civil Engineering Prog. METU NCC

I hereby declare that all information in this document has been obtained and presented in accordance with academic rules and ethical conduct. I also declare that, as required by these rules and conduct, I have fully cited and referenced all material and results that are not original to this work.

Name, Last name : Pelin Güven

Signature :

ABSTRACT

EXPERIMENTAL AND NUMERICAL ANALYSIS OF
A SALT GRADIENT SOLAR POND

Güven, Pelin
MSc. Sustainable Environment and Energy Systems Program
Supervisor: Asst. Prof. Dr. Onur Taylan
Co-Supervisor: Asst. Prof. Dr. Mehdi Amouei Torkmahalleh

September 2018, 86 pages

A salt gradient solar pond (SGSP) is a low-cost solar energy system, collects incoming solar radiation and then stores it in the form of thermal energy. SGSP has been developed recently and is considered as a large-scale energy collector for long-term use with no or little maintenance. It also has no environmental hazard. Most importantly, solar energy meets the energy demand in a clean and sustainable way; thus, SGSP can be though as a sustainable alternative for conventional energy systems. SGSP has three zones. The first zone, located right below the surface, is called Upper Convective Zone (UCZ), it has both the lowest temperature and density since it contains fresh water. The second zone is Lower Convective Zone (LCZ), this is where the solar radiation is stored, yielding the highest temperature and density. Finally, the third zone is Non-Convective Zone (NCZ), which is placed between LCZ and UCZ, including water with different concentrations of salt. Solar radiation is mostly absorbed in the LCZ, which results in increasing water temperature in this zone. To facilitate

the working principle of SGSP and store energy, it is very important to create and maintain temperature and density gradients. Temperature gradient depends on several factors, such as solar radiation, wind speed, and ambient temperature as well as the diameter of SGSP, and depth of each zone. The aim of this thesis is to investigate the experimental and numerical analysis of a solar pond. In the experimental analyses, performance evaluation of the solar pond is conducted based on experimental data, which includes solar radiation, wind speed, and ambient temperature. Based on the experimental analyses, it can be concluded that solar insolation, wind speed, and ambient temperature have coupled effects on pond temperature. Besides, it is known that obtaining high LCZ temperature is the main purpose of SGSP mechanism and during the experimentation, the maximum LCZ temperature was recorded to be 46ºC. According to the results, GHI has a more significant impact on controlling the temperature of the layers than ambient temperature and wind speed. After that, a numerical model is developed using the finite element method to conduct the parametric analyses to investigate each effect of parameters individually on the layer temperatures. Based on numerical results, UCZ and NCZ temperatures increase with increasing insolation, whereas LCZ mostly protects its temperature. Additionally, wind speed only affects UCZ temperature, and it does not a have profound effect on both NCZ and LCZ temperatures. The numerical results indicate that variation in ambient temperature has the highest impact on pond temperature among other variables. Besides, it is maintained that the diameter of SGSP does not affect the pond temperature. As future work, a more detailed transient model is required to examine the effects of layer thicknesses on pond temperature. Additionally, using transparent cover materials over the surface of the pond can be examined in detail; thus, the amount of stored sustainable energy in the lower layer might increase, which can directly increase the overall efficiency of a SGSP.

Keywords: Salinity gradient solar pond, solar energy, temperature gradient

ÖZ

TUZ KATMANLI GÜNEŞ HAVUZUNUN DENEYSEL VE SAYISAL ANALİZİ

Güven, Pelin
Yüksek Lisans, Sürdürülebilir Çevre ve Enerji Sistemleri
Tez Yöneticisi: Dr. Öğr. Üyesi Onur Taylan
Ortak Tez Yôneticisi: Dr. Öğr. Üyesi Mehdi Amouei Torkmahalleh

Eylül 2018, 86 sayfa

Tuz katmanlı güneş havuzu, düşük bütçeli ve güneş enerjisine dayalı bir sistemdir. Gelen güneş enerjisini toplar ve termal enerji formunda depolanmasını sağlar. Uzun süreli kullanımda yüksek ölçekli enerji depolayıcısı olarak görülmesiyle birlikte, az bakım gerektirdiği ve çevreye zarar vermemesinden dolayı son zamanlarda geliştirilmekte olan bir sistemdir. Güneş enerjisi, enerji talebini temiz ve sürdürülebilir bir şekilde karşılar; bu yüzden günümüzde çoğunlukla kullanılan enerji kaynaklarına sürdürülebilir bir alternatif olarak düşünülebilir. Tuz katmanlı güneş havuzu üç ana bölgeden oluşmaktadır. Birincisi, hemen yüzeyin altında bulunan üst konvektif bölgedir ve sadece sudan oluştuğu için en düşük sıcaklık ve yoğunluğa sahiptir. İkinci katman, alt konvektif bölge, en yüksek sıcaklık ve yoğunluğa sahip olmakla birlikte, güneş enerjisinin depolandığı katmandır. Sonuncusu ise, alt ve üst konvektif katmanlar arasında bulunan ve farklı tuz derişimlerine sahip olan, konvektif olmayan bölgedir. Çoğunlukla alt tabakada absorbe edilen güneş enerjisi o bölgedeki sıcaklığın yükselmesiyle sonuçlanır. Sıcaklık ve yoğunluk değişiminin oluşturulması ve kontrol

edilmesi, tuz katmanlı güneş havuzlarının çalışma prensibini anlamak açısından çok önemlidir. Elde edilen sıcaklık farkları; gelen güneş radyasyonuna, rüzgar hızına, hava sıcaklığına, buna ek olarak güneş havuzunun çapına ve her bir bölgenin derinliğine bağlıdır. Bu araştırmanın temel amacı, güneş havuzunun deneysel ve sayısal analizini incelemektir. Elde edilen deneysel verilere (güneş radyasyonu, rüzgar hızı ve hava sıcaklığı) göre güneş havuzunun performans değerlendirilmesi yapılmıştır. Deneysel analizlerde, gelen güneş ışığının, rüzgar hızının ve hava sıcaklığının birbirine bağlı olarak etkisi vardır. Bunun yanı sıra, tuz katmanlı güneş havuzunun temel amacı alt konvektif bölgede yüksek sıcaklık elde edebilmektir ve yapılan deneysel analizlere göre elde edilen maksimum alt konvektif bölge sıcaklığı 46ºC olarak bulunmuştur. Elde edilen sonuçlarda, güneş radyasyonunun katmanların sıcaklık değişimi üzerindeki etkisinin hava sıcaklığının ve rüzgar hızının etkisinden daha fazla olduğu gözlemlenmiştir. Daha sonrasında, gelen güneş ışığının, rüzgar hızının ve hava sıcaklığının etkilerini ayrı ayrı inceleyebilmek adına sayısal modelleme geliştirilmiştir. Elde edilen sonuçlara göre, üst ve orta katmanların sıcaklıklarının artan güneş radyasyonu ile artarken, alt katmanın genellikle sıcaklığını koruduğu gözlemlenmiştir. Buna ek olarak, rüzgar hızının sadece üst katmana etkisinin olduğu, orta ve alt katmanlarda önemli bir etkisinin olmadığı gözlemlenmiştir. Sayısal modelleme sonuçları, katmanların sıcaklığının değişmesinde en fazla etkinin değişen hava sıcaklığıyla elde edildiğini göstermiştir. Bunun dışında yapılan sayısal analizlerde, güneş havuzunun çapının artıp azalmasının katman sıcaklıklarında herhangi bir değişiklik yapmadığı bulunmuştur. Katmanların kalınlığının güneş havuzu sıcaklık değişimleri üzerindeki etkilerini daha iyi değerlendirebilmek için daha detaylı bir modelleme oluşturulması ilerideki çalışmalar için planlanmaktadır. Ek olarak, güneş havuzunun yüzeyini geçirgen maddelerle kaplamak detaylı bir şekilde incelenebilir; böylece alt katmanda depolanan sürdürülebilir enerji miktarı artabilir ve bu da doğrudan güneş havuzunun veriminin artmasıyla sonuçlanabilir.

Anahtar Kelimeler: Tuz katmanlı güneş havuzu, güneş enerjisi, sıcaklık değişimi

To My Family

ACKNOWLEDGMENTS

I would like to express my deepest gratitude to my supervisor, Asst. Prof. Dr. Onur Taylan and my co-supervisor Asst. Prof. Dr. Mehdi Amouei Torkmahalleh for their guidance, advice, constructive criticism, encouragement and insight throughout my research.

I would also like to thank my lovely parents Yurdagül and Aydın Güven, both of my grandparents Fatma and Nizamettin Özalp for all their efforts. I know that they are always with me. They were always supportive and wished the best for me. In short, I would like to thank all my family members for always being there for me and supporting me through hard times.

I would also like to thank Pevrin Harmanlı and my dear friends (especially; Beray Aydın and Ceren Yağmur Öztürk) for all their help, advice and suggestions throughout my MSc process.

The support of Middle East Technical University Northern Cyprus Campus,Campus Research Fund (Project No.: BAP-16-YG-3) is gratefully acknowledged.

TABLE OF CONTENTS

LIST OF TABLES

LIST OF FIGURES

CHAPTER 1
INTRODUCTION

1.1 Motivation

Energy is one of the most significant parameters of economic progress, and it can be observed that the energy demand is increasing rapidly (Amar, 2013). For instance, Kaygusuz and Toklu (2012) reported that the consumption of energy per capita shows both progress and level of modernity of a country. Fossil fuels, which are the most used energy sources in the world, have very harmful effects on the environment. Although these main energy sources menace the stability of the Earth, their consumption is increasing daily due to the developments in the industry and living standards, as well as the increase in world population (Meadows et al., 1993).

It is known that oil, coal, and natural gas are the main energy sources which are estimated to deplete in the next few decades (Twidell et al., 2015). Fossil fuels can create critical threats for the world, as burning fossil fuels emit carbon dioxide, which is a major greenhouse gas and causes climate change. Furthermore, air pollution, ozone depletion, forest destruction as well as radioactive emissions are other important problems caused by fossil fuels (Dincer, 2000). Alternative and renewable energy sources which cause less environmental hazards can prevent these problems. Nevertheless, it is important to understand that sustainable enhancement demands a sustainable supply of energy sources. Such resources need to be available at a reasonable cost and be used for all essential processes with having no negative environmental impact. At this point of view, renewable energy sources including sun and wind play an important role because they are abundant, and they can be considered as sustainable for a long-term period, whereas fossil fuels are mainly finite, and they have serious environmental issues. Therefore, Dincer (2000) suggested that the key component of sustainable development could be obtained by using renewable energy sources and technologies.

Renewable energy technologies such as wind turbines, photovoltaic cells, biomass plants, etc. are among the most effective and sustainable solutions for the

environmental problems. Nowadays, new policies and technologies are being investigated by industrialized countries for achieving sustainable energy in the future, focusing on the renewable energy sources. However, renewable energy sources are variable or intermittent, such that, these systems cannot always meet the electricity demand, unlike the conventional power plants. According to Dell et al. (2001), variations in the renewable energy production may cause instability in the power network and cause demand imbalance. Therefore, energy storage technologies can be considered as one of the solutions to this issue.

Energy storage does not only suggest a solution to the variability issue but also allows to increase the renewable energy utilization in the energy generation mix, thus, yields to a more sustainable environment. Furthermore, it is crucial to understand that energy storage technologies are necessary for balancing the supply and demand. The demand for power changes with time and it directly affects the price of electricity. During peak demand times, when the consumption of electricity is generally higher than the average consumption, price will become higher. For example, coal-fired and nuclear power plants, which are flexible forms of energy production, can meet this demand; however, coal-fired ones have serious impacts on the environment. With this viewpoint, it may be deduced that sustainable energy storage technologies play a crucial role since they have less environmental hazards.

One of the most important renewable energy sources in the world is solar energy. It is clean and abundant which can be considered as a suitable alternative to conventional energy sources. However, as mentioned before, the usage of solar energy is restricted since it is not only time-dependent but is also an intermittent energy source. Therefore, the main difficulty is to meet the energy demand while storing the solar energy. At this point, the concept of salinity gradient solar ponds, which are the integral devices used to collect and store the solar energy, are significant solutions for this challenge (Goutham et al., 2013). Containing different amounts of salt, which are heated by the absorption of the solar energy and supply long-term thermal storage, is the general definition for the solar pond (Suárez et al., 2010). In other words, they collect solar energy and store it in the formation of the thermal energy, therefore, they can be considered as large-scale energy collectors having low cost of solar energy system. Moreover, Salt Gradient Solar Pond, henceforth SGSP, requires little maintenance and

most importantly, they have little or no environmental hazards. Salt concentration in the pond increases through the bottom of the pond where the useful solar energy is trapped (Dincer et al., 2012). Hence, it is not only cheap but also an effective way to store solar energy.

1.2 Objectives

As mentioned in the motivation section, solar energy is one of the most effective ways of renewable, clean, and sustainable energy. SGSPs are used for storing the incident solar energy in the formation of different concentrations of salty water especially for the processes of low-temperature heat sources. Furthermore, the main aim of this mechanism is to store and collect thermal energy at the bottom layers of the pond. Since its mechanism depends on clean and renewable energy, SGSP can be thought of as a sustainable alternative for the conventional power plants, which are mainly used for non-clean energy sources to produce an electricity like fossil fuels.

In this thesis, experimental and numerical analyses of a salinity gradient solar pond are going to be investigated.

Performance evaluation of the solar pond will be conducted based on experimental data. For instance, to investigate the temperature distribution at different heights of the pond, plot of temperature versus height of the solar pond is created. Additionally, by using the distribution of layer temperatures including UCZ and LCZ, solar radiation, wind speed, and ambient temperature versus a specific time duration is created to examine the effects of weather conditions, including incoming solar radiation, wind speed, and ambient temperature, on the layer temperatures. However, all of them collectively affect the layer temperatures, which is the main difficulty of the experimentation. Finally, efficiency of the pond will be calculated.

To investigate each effect individually, modeling in COMSOL is developed under the parametric study. Additionally, investigation of pond geometry including diameter, and layer thicknesses of a solar pond will be examined. Besides, validation of numerical modeling temperature results will be compared with the temperatures of the experiment.

1.3 Organization of Thesis

This thesis is composed of 5 chapters. Chapter 1 summarizes brief introductory information about both conventional energy sources and renewable energy sources. Additionally, the importance of using solar energy as a part of renewable energy sources is mentioned. Moreover, general concept of salt gradient solar pond is addressed. Chapter 2 consists of four parts that include brief literature survey about the thesis topic. In Section 2.1, the working principle of a salt gradient solar pond is briefly examined. Moreover, in Section 2.2, experimental studies about the SGSP are examined such as effects of salt, whereas in Section 2.3, dimension effects are discussed as part of numerical studies. Furthermore, some significant heat extraction methods from SGSP are investigated in Section 2.4. Chapter 3 contains information about the experimental methodologies applied in this thesis, and then in Chapter 4, experimental results are given and discussed. Similarly, numerical methodologies applied in this thesis is mentioned in Chapter 5, and the major findings of the numerical part are addressed in Chapter 6, which consist of three main parts. Finally, conclusions highlighted and suggestions for the future research are addressed in Chapter 7.

CHAPTER 2
LITERATURE SURVEY

2.1 Working Principle of Salt Gradient Solar Pond

Solar ponds consist of three main layers. The schematic view of a salt gradient solar pond can be seen in Figure 2.1. The top layer, which is known as the upper convective zone, UCZ, is located at the top of the pond sharing an interface with ambient air and it contains fresh water only. It has the lowest temperature, which is around the ambient temperature, and its density is close to the density of fresh water to provide the purity of the pond (Dincer et al., 2012). Stability of UCZ is impacted by surface winds and evaporation because of its location. Therefore, it is important to compensate for evaporation loss to protect working stability of the pond (Srinivasan, 1993 and Monjezi et al., 2016).

The second layer is called the non-convective zone (NCZ), which is also known as the thermally insulating layer, comprises of a salinity gradient. The concentration of salty water, as well as the temperature at this layer, increases with the depth. In other words, concentration of the water that is close to the surface is less dense than the water that is close to the bottom layer of the pond (Monjezi et al., 2016). The water in this layer cannot rise or sink since it is lighter than the lower layer, whereas it is heavier than in the surface layer. Therefore, it suppresses convection and behaves as an insulator to prevent heat diffusion from the lower layer to upper layer (Valderrama et al., 2016).

Furthermore, this zone is much thicker than the surface zone. Generally, it accounts for more than half the depth of the solar pond. The thickness of the insolation zone must be adequately adjusted because if the thickness is too high, transmission of solar insolation decreases, whereas if it is too low, it might cause high heat losses (Sukhatme et al., 1996). NCZ allows solar radiation to access the lower zone, while also preventing the escape of long-wave solar radiation.

The last layer is the lower convective zone, LCZ, which is also recognized as the heat storage zone, has the highest temperature and density. Not only concentration but also temperature is constant through this layer. The sturdiest thermal interaction can be

observed at this layer due to its high temperature. Thus, a considerable part of the incoming solar radiation storage can be seen in this part. (Dincer et al., 2012). To obtain a dynamically stable mechanism, adding brine regularly to the lower layer due to the diffusion of salt through to the UCZ is substantial (Akbarzadeh et al., 2009). Alternatively, Torkmahalleh et al. (2017) suggested adding salt to the bottom of LCZ during the installation of the pond instead of regularly adding brine to the LCZ.

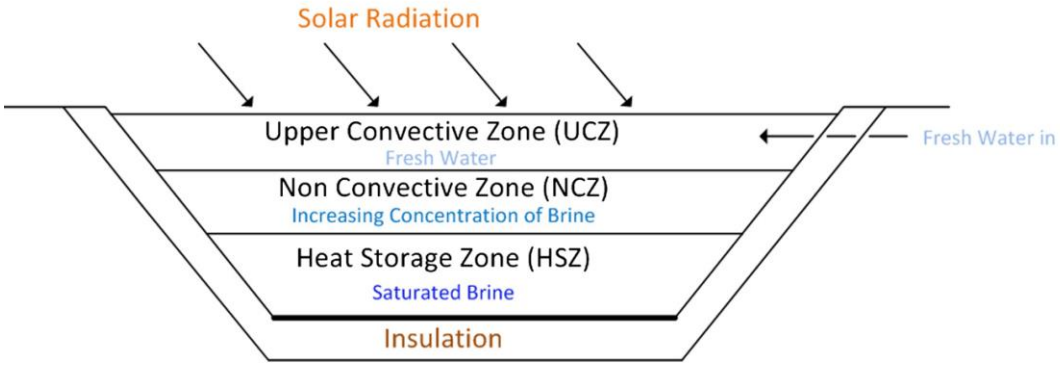

Figure 2.1. Three zones of a typical salt gradient solar pond (Monjezi et al., 2016).

It was reported that nearly 30% of incoming solar radiation could reach a depth of 2 meters in a clear natural pond. This solar insolation can be absorbed in the bottom layer of the pond. Generally, natural pond cannot reach higher temperatures than the ambient temperature since hot water at the lower layer becomes lighter and rises through the surface layer; thus, heat loss can be observed through the ambient air. Therefore, it is important to prevent mixing between these layers to obtain higher temperatures of the lower layers. This temperature gradient can be accomplished by adding salt to the lower layers, which results in making lower layers denser than the upper layer. For example, magnesium chloride and sodium chloride are the most common salts to be added to the pond to avoid mixing between the upper and bottom layer due to their low costs. Additionally, using a transparent honeycomb structure, which consists of a transparent plastic material, is also used to prevent mixing since it traps stationary air and supplies good transparency to solar radiation as wells as cutting down loss from the pond (Srinivasan, 1993).

There are major factors that play a significant role in the working performance of the salt gradient solar pond, given that SGSP collects solar irradiation and stores it as the thermal energy. Hence, not only thermal efficiency but also thermal performance is very significant.

The heat, which is removed from the solar pond, and the solar energy that penetrates the top surface of the SGSP at a specified time, are two essential parameters for thermal efficiency due to their ratio being used to define the thermal efficiency. (Angeli et al., 2006).

Additionally, Andrews and Akbarzadeh (2005) defined the thermal efficiency as below:

$$\eta = \frac{C[T_p(d) - T_a] + \dot{q}}{\bar{H}} \quad (1)$$

According to this equation, the denominator includes the average flux of incoming solar radiation that incident on the surface of SGSP is represented as $\bar{H}$ (W/m^2), while numerator consists of two parameters. One of them is the rate of heat transfer per unit area of the pond, which is shown as $C[T_p(d) - T_a]$. In this part, C (in W/K/m^2) is the heat capacity rate per unit area of the pond, and $T_p(d)$ is the bottom of gradient layer's temperature, d represents the thickness of NCZ, and the ambient temperature is demonstrated as T_a (in °C). Another term is $\dot{q}$ showing the rate of heat extraction from the LCZ per unit area (in W/m^2) (Andrews and Akbarzadeh, 2005).

Absorption on the LCZ, heat loss on the surface layer, thicknesses of each layer, heat loss around the pond such as bottom or side losses, as well as solar insolation are the major aspects that impact the thermal efficiency. It is known that the thermal performance of the SGSP is subject to solar radiation accessing the LCZ where the solar energy is stored (Beniwal et al., 1987). Thus, the maximum energy efficiency can be seen in the LCZ when it is compared to the other parts of the pond since the storage of the energy can be maintained in this zone. Nevertheless, in the UCZ, as mentioned before, because of its position, it is mostly mixed by both surface winds and evaporation, thus; the largest heat loss, as well as the lowest efficiency, can be observed in this zone (Nalan et al., 2011).

Moreover, transparency is also an important aspect of the thermal efficiency of the pond, which can be affected by the formation of the algae as well as dust. Thus, protecting the clarity of the pond is significant and the growth of algae can be prevented by adding chemicals such as bleaching powder or copper sulfate. According to Srinivasan (1993), it was reported that accumulation of dust does not affect the absorptivity of incoming solar radiation at the bottom layer but flowing of dust can be adjusted by adding alum.

Therefore, salinity distribution, temperature distribution, pond clarity, weather conditions, heat loss and rate of heat extraction are the main factors affecting the performance of a solar pond (Chinn et al., 2003).

2.2 Experimental Studies

Many studies have investigated the impact of different types of salt on solar ponds. It is important that salt should not contain harmful chemicals that have a potential to pollute groundwater and air, so that they would be environmentally friendly (Kumar et al., 2016). For example, research focusing on the detrimental effects of salts on the environment shows that the ammonium types of salt such as sulphates, nitrates, chlorides or phosphates are not hazardous for the environment (Berkani et al., 2015).

Moreover, the solubility of salts must be stable, and it should not vary significantly with increasing temperature. For example, after adding a specific amount of NaCl in a solution, the salt will not dissolve. At this point, salt reaches its solubility limit and solution gets saturated in NaCl. Kumar et al. (2016) claimed that sodium chloride, magnesium chloride, and sodium sulphate are the most favored salts due to their stable solubility ranges, as shown in Figure 2.2.

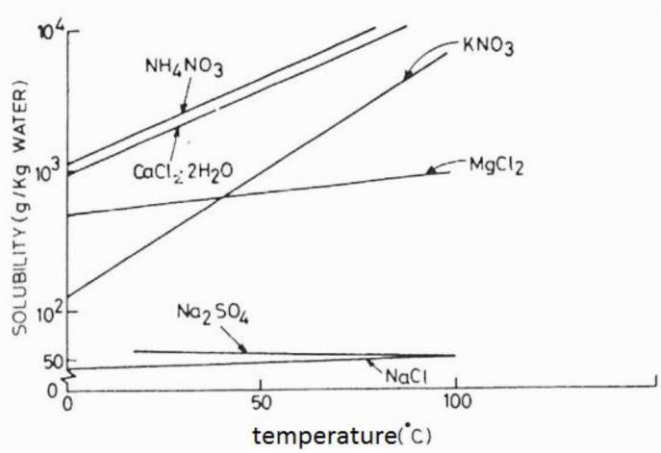

Figure 2.2. The solubility of different salts with temperature (Kumar et al., 2016).

Furthermore, to store high amounts of solar energy, solubility of salt in water should be transparent to allow solar radiation to the bottom layers of the ponds. In addition to these, molecular diffusivity of salt should be low to provide the stability of the pond. Another important feature is the cost; it should be both available and cheap (Kumar et al., 2016).

Berkani et al., (2015) investigated the performance of three different solar ponds having various types of salts including NaCl, Na_2CO_3, and $CaCl_2$ between the period of 1 and 29 June 2013 in Algeria.

K-type thermocouples were used in this experiment. In addition to that, digital thermometers were located on the outside of the pond which were used to measure the ambient temperature. Temperature was recorded every three hours for the experiment. During the process, due to the evaporation, replenishment of UCZ was done properly; thus, the height of this zone remained nearly the same for each pond.

It was found that $CaCl_2$ pond has the fastest response with increasing temperature, which can be seen in Figure 2.3. However, temperature of $CaCl_2$ pond reduces quickly in the condition of no insolation. Table 2.1 shows the highest temperature values measured in these ponds during the period of 28 days. Moreover, NaCl showed higher temperature rise than (9.7%) Na_2CO_3, while the pond including $CaCl_2$ reached a temperature value which was 14.41% higher than Na_2CO_3 pond. This may be due to the differences in their heat capacity values per unit volume. The smallest value is registered to calcium chloride. As a result, solar pond containing calcium chloride showed a good chance for heat storage (Berkani et al., 2015).

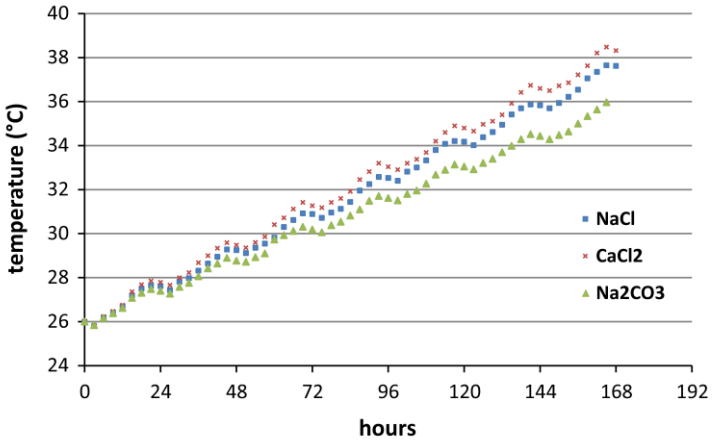

Figure 2.3. Temperature profiles of three ponds during the first week (Berkani, 2015).

Moreover, it is known that solar insolation absorption, accessing the bottom layer of the SGSP, can be affected adversely by the formed crystals; thus, it is significant to avoid the formation of crystallization. For example, since $CaCl_2$ solution at LCZ might be used far from its saturation point, it could be usable with a small risk of salt crystallization. Although NaCI is the most common salt used in these applications due to its availability and low cost, this study shows that not only Na_2CO_3 but also $CaCl_2$ can be used in solar pond applications (Berkani et al., 2015).

Another study brought a different aspect about the salts, which focused on the performance of magnesium chloride ($MgCl_2$) at an experimental 15 m^2 solar pond, having circular polyethylene tank with 4.4 m diameter, 2.0 m height, and 0.008 m wall thickness, built in Australia in June 2002 (Chinn et al, 2003). Bittern consists mainly magnesium chloride, a waste product of salt processing plant, which is nearly 10% denser than sodium chloride. Furthermore, it has a powerful salinity gradient as well as it is a cheaper alternative than a sodium chloride pond.

During this experiment, regular salt replenishment in the LCZ and surface washing in the UCZ was done properly, since it can correct instabilities occurring in the pond. Density meter, digital thermometer, and turbidity meter were used in this experiment. The density meter is generally used to measure the density of liquids where the effect of oscillation frequency is calculated and converted to density. It also has a temperature sensor, giving a reading of the sample density at its sample temperature, allowing the measured density to be corrected to pond temperature. Moreover, using a digital thermometer, temperature profile of the pond was maintained. The temperature profile

of the pond shows the thermal performance of the pond, and it is required for measuring sample density corrections. To maintain an effective thermal performance of the pond, water clarity plays a significant role and turbidity meter is used for measuring water clarity. UCZ should have good water clarity since it provides a higher percentage of solar radiation to penetrate through the lower layers of pond, and thereby helping a higher amount of heat to be stored in the LCZ. In this experiment, six T-type thermocouples were used. Temperature profiles obtained from these thermocouples show the performance of magnesium chloride solar pond. The maximum and minimum temperature values of $MgCl_2$ pond can be seen in Table 2.1. Furthermore, average efficiency was calculated as about 9% from this experimental pond during a period of 10 months. Hence, it is possible to establish a solar pond with bittern based on pond observations and data collection from 15 m^2 magnesium chloride solar pond. This is because approximately 25°C temperature difference could be provided during colder months. Moreover, it was seen that at higher temperatures, bittern protects its stability since no erosion was observed between the LCZ and NCZ interface (Chinn et al., 2003). Therefore, bittern might be a viable alternative to sodium chloride pond, since it generates not only stronger but also shows more stable gradient. Furthermore, used as a waste product in the salt production process in salinity-stricken areas can increase its chance to be preferred based on Chinn's (2003) study.

Table 2.1. Characteristics of Experimental Solar Ponds.

Location	**Diameter (m)**	**Height (m)**	**Salt**	**T_{max} (°C)**	**T_{min}(°C)**	**References**
Australia	4.4	2.0	$MgCl_2$	78.5 (LCZ) 36.3 (UCZ)	35.0 (LCZ) 6.50 (UCZ)	Chinn et al. (2003)
Algeria	1	1	NaCl	72.0	~28.0	Berkani et al. (2015)
Algeria	1	1	Na_2CO_3	65.6	~26.0	Berkani et al. (2015)
Algeria	1	1	$CaCl_2$	75.1	~28.0	Berkani et al. (2015)

Additionally, Kurt et al. (2006) investigated the density gradient of a small-scale solar pond using sodium carbonate salt (Na_2CO_3). During this experiment, a solar simulator was used to provide the solar radiation that was placed about 35 cm above the surface of the pond. This study was investigated under laboratory conditions by using SGSP with dimensions of 60 x 50 cm^2 as well as 60 cm height. The thickness of the pond layers was adjusted as 10 cm for the surface layer, 25 cm for the gradient zone and 25 cm for the lower convective zone. In this experiment, K-type thermocouples were used at eight different locations to obtain correct temperature readings.

This study examined the suitability of SGSP using Na_2CO_3 salt; hence, four experiments including varying ranges of concentration gradients, adjusted as 8%, 10%, 12%, and 16% were conducted under laboratory conditions. Based on the four experimental results, both temperature and density profiles with respect to the depth of pond were created. The maximum salinity percentage difference between the surface layer and bottom layer was obtained in the fourth experiment which was adjusted as 16% and due to the formation of the crystal solids at the pond, salinity levels higher than the 16% could not be reached.

Furthermore, based on obtained density and temperature plots, results of the third and fourth experiments were more stable than the other experiments with respect to the pond depth. Additionally, it was observed that the salinity percentage of 12% (3^{rd} experiment) is necessary to prevent convection between the bottom and upper layer. Therefore, salinity level about 12% might be necessary to store the incident solar radiation using Na_2CO_3.

Moreover, temperature difference between the upper and bottom layer was measured to be approximately 10°C after one-week of observations based on the 3^{rd} experiment, which can be seen in Figure 2.4. Because a solar simulator was used, a small portion of radiation reached slowly through the lower layers whereas a great portion of incoming radiation was absorbed in the surface layer, and therefore, the temperature of UCZ increased more quickly than the other layers. Thus, a larger-scale amount of incident radiation can be utilized as stored energy at the bottom layer of the pond, when the proper density gradient with Na_2CO_3 is maintained (Kurt et al., 2006).

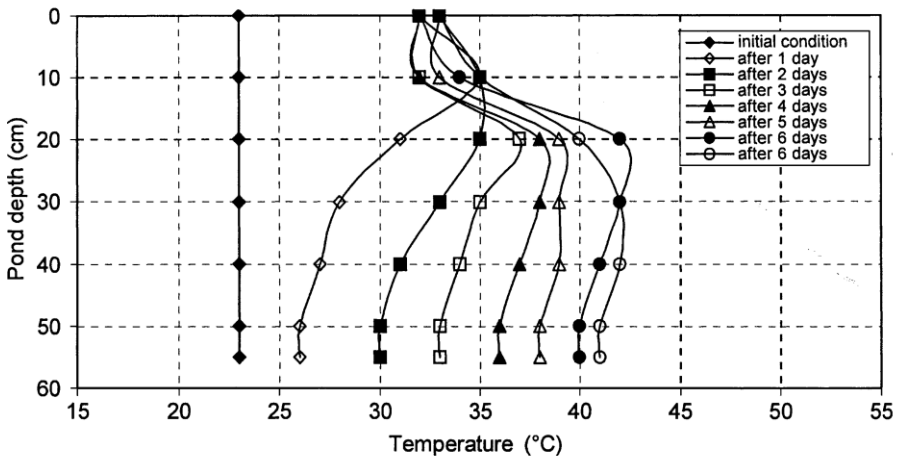

Figure 2.4. Pond depth versus temperature profile for the third experiment (Kurt et al., 2006).

2.3 Numerical Studies

Angeli et al. (2004) investigated the impact of the insulated layer, NCZ, the thickness on the amount of energy storage in the lower convective zone by using a 1-D finite difference semi-implicit model. Most of the incoming radiation can be absorbed by both surface and insulated layers before it reaches LCZ, and since energy distributed through the ground and insulated zone, solar energy that can reach the LCZ is not completely accessible. Therefore, thicknesses of the NCZ should be adjusted properly. Based on their results, the temperature of the LCZ increases with the increasing thickness of NCZ. For instance, if the optimum thickness is adjusted approximately 2.5 m, maximum temperature can nearly reach to 90°C, whereas when the thickness of NCZ is modified to 1 m, 40°C of LCZ is obtained. Furthermore, ideal heat storage efficiency versus LCZ temperature was plotted and based on this, heat storage efficiency decreased with the increasing temperature of LCZ, since increasing temperature has resulted in the increasing heat loss through the NCZ (Angeli et al., 2004).

Garmana et al. (2008) also investigated the parameters such as layer thicknesses of a solar pond, which serves for the water desalination unit by using a mathematical model. It is known that the thickness of a surface zone, UCZ, which is exposed to surface wind effect, should be arranged properly. If its thickness increases, the amount of solar radiation that reaches the lower zones decreases. Based on this study, 0.3 m was found as the minimum thickness for the UCZ to protect pond from severe weather

conditions. Furthermore, the thickness of NCZ is also significant since it affects directly the solar radiation that can reach the LCZ. When the thickness of NCZ increases, its insulation quality increases whereas solar radiation reaching the LCZ decreases. Depending on their results, 1.1 m was found as an optimum thickness for NCZ since below this value, temperature cannot reach 60°C, which is necessary to start the desalination unit, and the minimum area can be obtained at this value. Additionally, 4 m is calculated as the optimum thickness for the NCZ because it requires the lowest surface area for the solar pond (Garmana et al., 2008).

Beniwal et al. (1987) examined the thermal efficiency of a SGSP by using a numerical model at varying functioning conditions, ($\Delta T/\widehat{H}$). ΔT represents the temperature difference between LCZ and ambient air, while $\widehat{H}$ shows the average incoming solar radiation that incident on a surface of the SGSP. As mentioned before, the layer thickness is important for the performance of the pond. According to Beniwal et al. (1987), thermal performance and the thermal efficiency increases with decreasing thickness of the UCZ, which can be seen in Figure 2.5. Based on this figure, the lowest efficiency that is close to 15%, is obtained when the thickness of UCZ is equal to the highest thickness of 0.5 m, whereas maximum efficiency, about 20%, is maintained when the thickness of the UCZ has the lowest value at 0.1 m., at the same operating conditions ($\Delta T/\widehat{H}$) as 0.25 °C m^2 W^{-1}. Likewise, if the thickness of LCZ increases, the thermal efficiency of the pond reduces since the amount of heat loss through the edges of the pond increases.

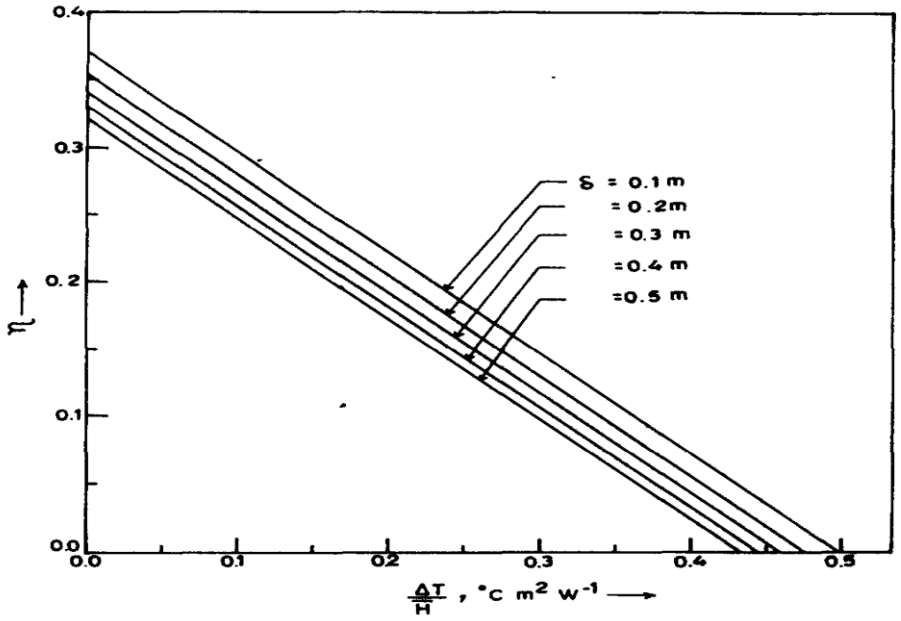

Figure 2.5. Thermal efficiency variations at different operating conditions and thickness of UCZ (Beniwal et al., 1987).

Furthermore, if the thickness of NCZ increases, the amount of solar insolation which is absorbed in this layer increases, and solar insolation that reaches the LCZ decreases; thus, efficiency reduces. Variations of the optimum thickness of NCZ at different operating conditions can be seen in Figure 2.6. For the condition of the thickness of the surface layer, δ, is equal to 0.2 m, the optimum z_1 value representing the thickness of the gradient layer can be found at about 2 m, and about 23% of maximum efficiency is obtained. Moreover, it can be easily seen that z_1 increases with the increasing δ and similarly optimum NCZ thickness increases with the increase different operating conditions, ($\Delta T/\widehat{H}$). As a result, not only maximum efficiency but also the optimum thickness of NCZ depends on both width of the surface layer and the operational conditions.

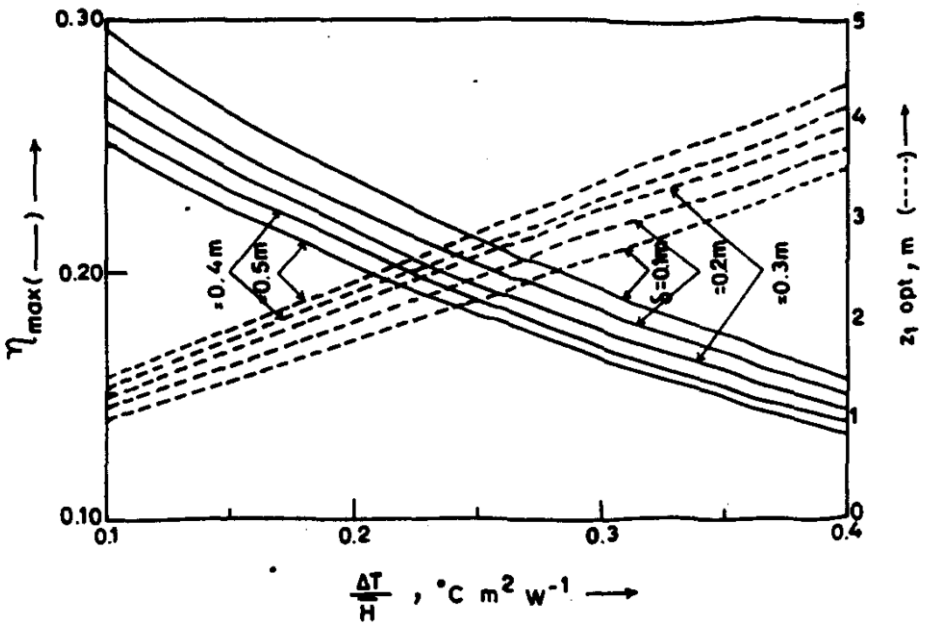

Figure 2.6. Variations between the maximum efficiency and the optimum thicknesses of NCZ (Beniwal et al., 1987).

Jubran et al. (2004) investigated the effects of not only tilt angle of the wall but also salt concentrations on the features of the layers using a numerical model, named as 3-D volume method. To decrease both heat loss through the ground and impact of shadows, sloped wall solar ponds could be used, but absorption of heat on these walls can change the stability of the gradient zone. In this study, two different models including a vertical wall and inclined wall were created shown in Figure 2.7. There are two layers for these models containing air and gradient layer.

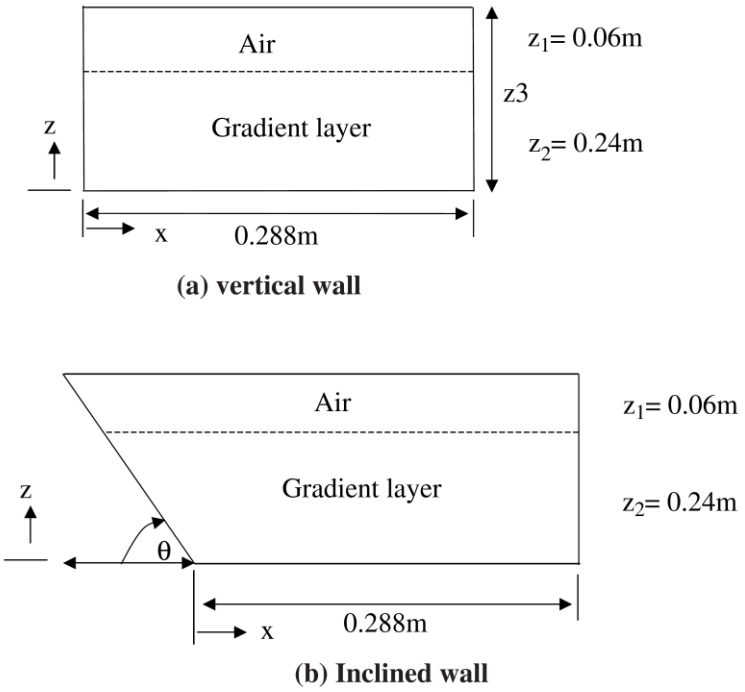

Figure 2.7. Vertical and inclined walls (Jubran et al., 2004).

For the gradient layer, using sodium chloride, salinity level changed from 0% to 8.24% at a constant temperature of 20°C, and each coefficient such as thermal conductivity, specific heat or thermal expansion were constant. Tilt angles were adjusted to 30°, 45°, and 90°. According to their results, it was observed that convective layers expanded after they were heated. The greatest expansion was observed when the tilt angle was equal to 30°, whereas the smallest expansion was obtained at an angle of 90°, which is illustrated in Figure 2.8. If the angle and horizontal contribution reduces, heat transfer rate also decreases, hence fluid temperature and heated wall temperature difference starts to increase which is resulted in raising the distance covered by layers. For instance, when there is high solar insolation, it would be better to use higher angles to prevent the movement of gradient layers. Therefore, tilt angles of the wall play an important role in the movement of the convective layers since their movement grows with reducing tilt angle.

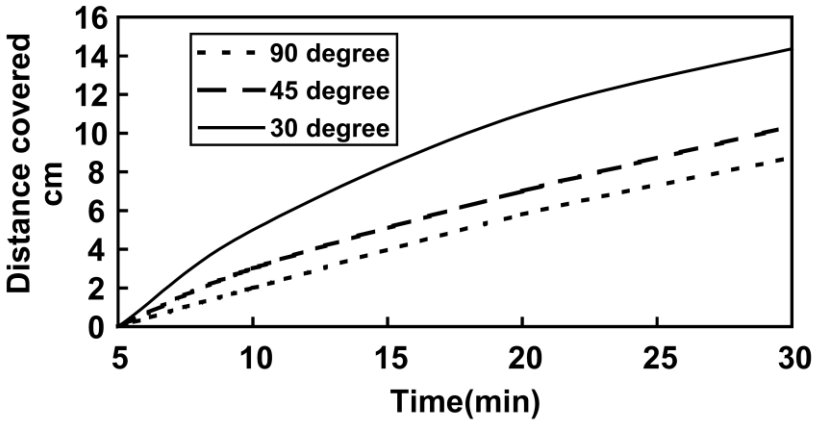

Figure 2.8. Distance covered of convective layers based on different tilt angles including 30°, 45°, and 90° with respect to time (Jubran et al., 2004).

Furthermore, salinity level has an influence on the characteristic of the convective layers. In other words, when the salinity level increases, not only thickness but also length of the convective layers reduce. For example, the fluid including a lower salinity level can move faster than the fluid with higher concentration. Hence, the higher stability of the SGSP can be maintained by increasing salt concentrations since it helps to reduce the activity of convective layers (Jubran et al, 2004).

Another study, which was investigated by Boudhiaf et al. (2012), mainly focused on problems related to hydrodynamics, both mass and heat transfer as well as stability of a SGSP. This research displays the significance of the thickness of NCZ and the influence of buoyancy ratio on the consistency of the pond. Their numerical model assumes Prandtl number and Schmidt number to be 6 and 1000, respectively, which are conformed to the features of salty water. The study concluded that when the buoyancy ratio was zero, as the fluid moved only due to thermal buoyancy force, storing incoming solar radiation in LCZ was very difficult. Therefore, hot water started to move through the upper layer and during this motion, heat loss was observed due to evaporation, radiation or heat by convection. Simultaneously, cold water, which was getting heavier, moved through bottom layers; thus, not only heat loss but also continuous mixing could be observed. Nevertheless, when the buoyancy ratio was equal to 10, convection movements could be constrained in the lower zone, and solar energy could be stored in LCZ. Moreover, stable salt concentration could be obtained when the buoyancy ratio is 10. Effect of buoyancy ratio on the dimensionless average

concentration between the layers can be seen in Figure 2.9. Based on this figure, when the buoyancy ratio increases, concentration in the UCZ closes to zero, while it reaches approximately one in LCZ.

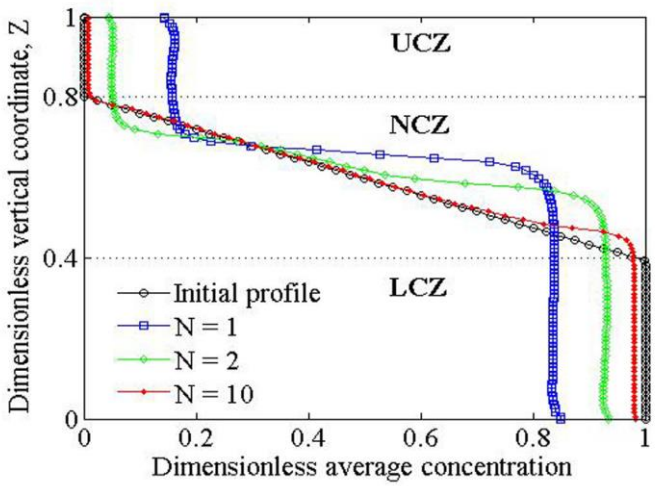

Figure 2.9. Average concentration profile with different buoyancy ratios (Boudhiaf et al., 2012).

Moreover, the temperature of UCZ decreases with increasing buoyancy force, while the temperature of LCZ increases as illustrated in Figure 2.10, which shows the effect of buoyancy ratio on the temperature of both UCZ and LCZ.

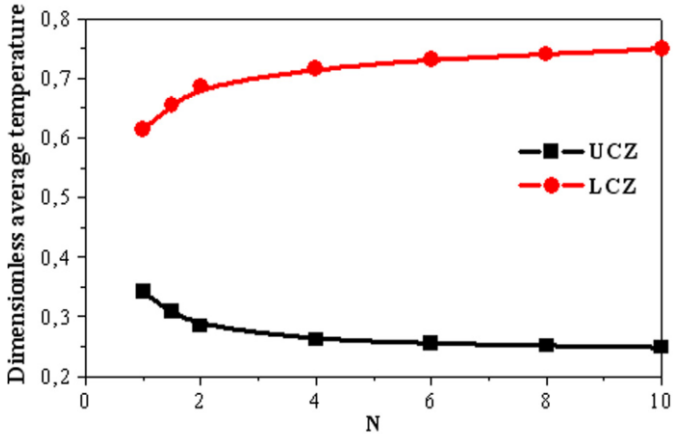

Figure 2.10. Impact of buoyancy ratio on the temperature of surface and bottom layer (Boudhiaf et al., 2012).

Furthermore, this study showed that if the thickness of the surface layer increases, higher temperatures can be obtained. However, increasing thickness of UCZ reduces the solar radiation that reaches through the bottom layer; thus, it should be adjusted properly. Additionally, increasing thickness of NCZ shows better insulation property

as well as preventing heat loss, whereas decreasing the thickness of energy storage zone results in the increasing temperature in LCZ, which can be seen in Figure 2.11.

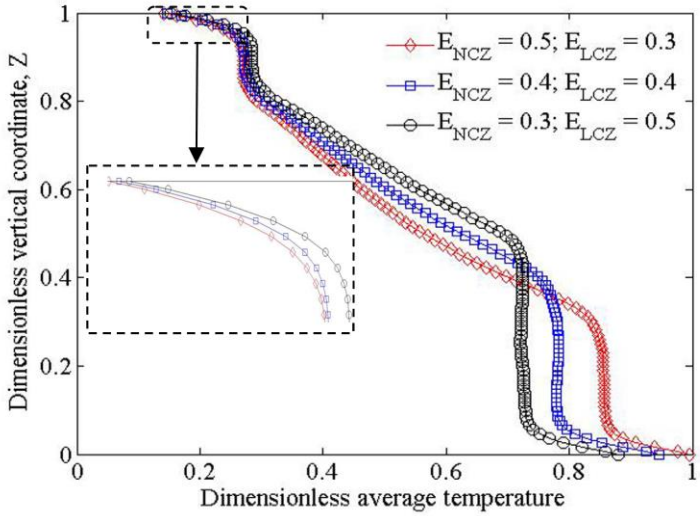

Figure 2.11. Impacts of varying thicknesses of LCZ and NCZ on the dimensionless average temperature when the buoyancy ratio is equal to 10, and assuming Pr=6, Sc=1000 (Boudhiaf et al., 2012).

Hence, thickness of non-convective zone is critical since it can prevent heat loss through the upper layer and provide an increasing temperature of the lower convective zone (Boudhiaf et al., 2012).

2.4 Heat Extraction Methods from SGSP

It is known that most of the solar insolation is initially absorbed in the UCZ. Nevertheless, a part of the absorbed heat by UCZ is lost due to both radiation and convection heat transfer. The remaining part of solar radiation can reach down to LCZ. It is known that solar energy is mostly stored in LCZ; thus, the temperature of bottom layer rises significantly. Hence, approximately 55°C temperature difference between the UCZ and LCZ can be maintained. Additionally, heating buildings, power generation as well as desalination aims can be evaluated by using this stored thermal energy (Tundee et al., 2010).

Many studies investigated the methods of heat extraction from the SGSP. For example, one study focused on a combined heat extraction obtained by both LCZ and NCZ. It has resulted in enhancing thermal efficiency level by up to nearly 50%, compared to

the heat extraction obtained by LCZ. Tundee et al. (2010) examined the heat extraction method using thermosyphons. Additionally, the comparison of the results by thermal simulations and experimental data maintained from SGSP was evaluated.

In their experimental setup, a solar pond with an area of 7 m^2 and depth of 1.5 m, in Thailand was operated. The daily temperatures and rate of heat extraction were examined. Temperature values were recorded using K-type thermocouples that were equally placed in the SGSP, and incoming solar irradiation was verified by a pyranometer. In this experiment, heat pipe heat exchanger, HPHE, was employed for heat extraction as shown in Figure 2.12.

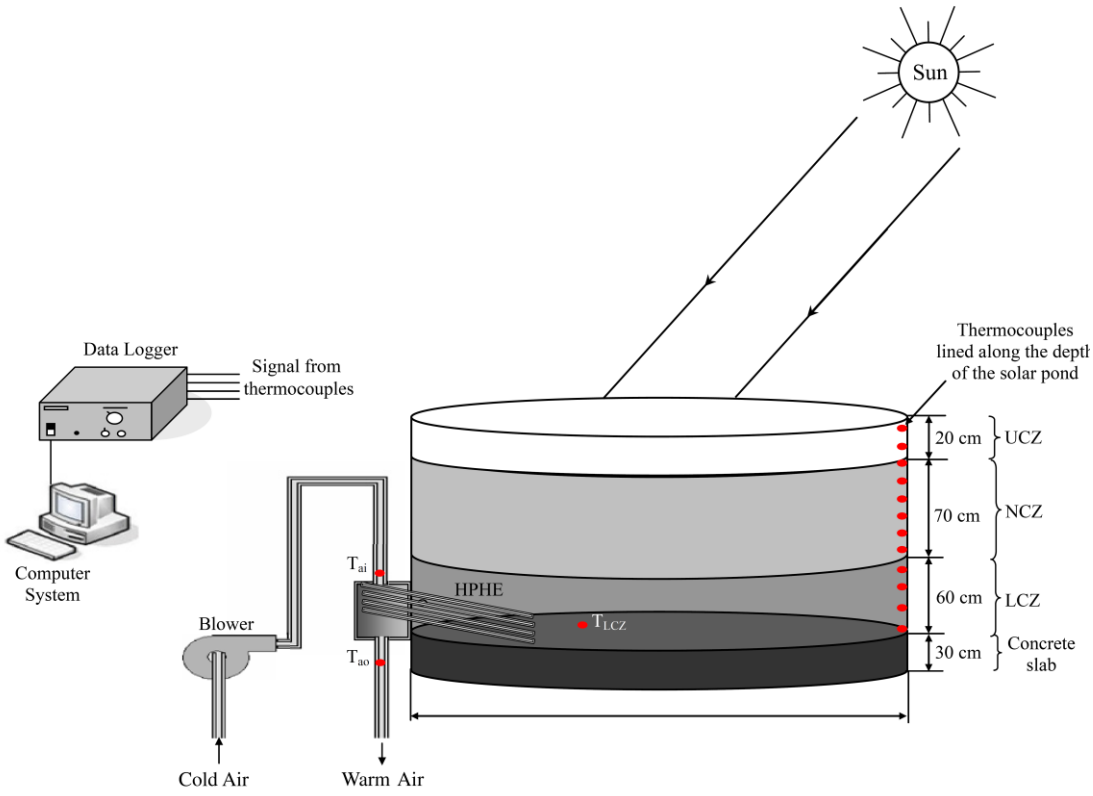

Figure 2.12. Experimental setup of SGSP and HPHE system (Tundee et al., 2010).

HPHE was composed of approximately sixty thermosyphons that were prepared with copper tubes. R134a known as tetrafluoroethane was chosen as heat transfer fluid. Moreover, the tilt angle of HPHE was adjusted to 60°, which was considered as an optimum angle for the setup, to increase the thermal performance of the SGSP. Tilting is an important aspect of providing heat transfer to reach essential parts of heat extraction systems including an evaporator and condenser. Generally, tilt angles higher

than 45° is preferred. However, the tilt angle of 90° resulted in the blockage of the condensation area with a liquid film. Thus, optimization of the tilt angle is essential. Circulation of the ambient air to the condenser was provided by a speed blower to extract heat from the lower convective zone. Rate of heat extraction was determined by the knowledge of both inlet and exit air temperature of the condenser as well as the volume flow rate. This experimental setup has been working since 2008, but heat extraction method using HPHE system was applied only in the summer of 2008. On 17th of June, the maximum LCZ temperature was obtained at 42°C, while the minimum bottom layer temperature was recorded at 32°C on February 7th. Moreover, the lowest ambient air temperature was also recorded on February 7th. It is known that solar insolation is a significant parameter for heat transfer; however, it is affected negatively with increasing thickness of LCZ. In other words, higher amounts of stored energy can be maintained with increasing LCZ thickness. Nevertheless, faster response time due to the varying weather conditions and incoming solar irradiation can be achieved with a small LCZ thickness (Tundee et al., 2010).

Furthermore, if the LCZ temperature is not high enough, low thermal performance is obtained by thermosyphon, since working fluid shows high thermal resistance at lower temperatures. However, at high temperatures, HPHE displays greater thermal performance. Therefore, higher heat extraction that is maintained by LCZ increases with higher temperatures using thermosyphon based heat exchanger. In addition, thermal performance depends on the number of transferring unit as well as air velocity. Simulation results showed that when the velocity of air decreased from 5 m/s to 1 m/s, thermal performance of the thermosyphon heat exchanger increased from approximately 28% to 43%, which can be seen in Figure 2.13. Thus, both air velocity and the number of transferring units can affect the effectiveness of a SGSP.

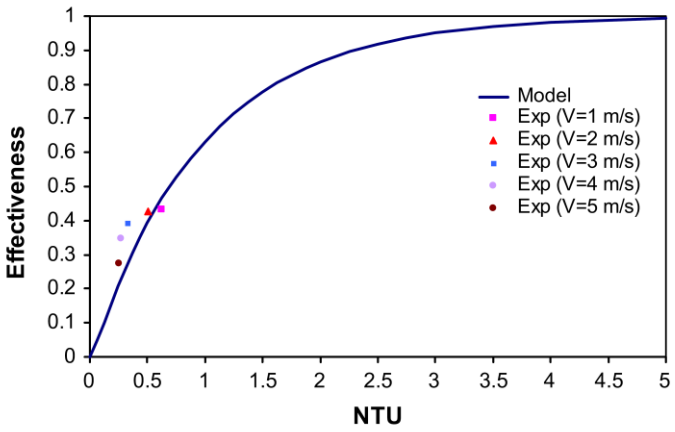

Figure 2.13. Thermal performance versus number of transferring units for the HPHE (Tundee et al., 2010).

Approximately 100 W heat extraction rate was obtained by using thermosyphon heat exchanger and the maximum effectiveness level reached up to nearly 45% for the heat exchanger when entering air velocity was adjusted to 1 m/s (Tundee et al., 2010). As a result, low air velocity is resulted in not only increasing heat transfer effectiveness but also decreasing power consumption by the air blower (Tundee et al., 2010).

Another study, which was conducted by Leblanc et al. (2011), investigated two main conventional heat extraction methods showing important examples, including El Paso and Pyramid Hill SGSPs. One of the important methods for heat extraction from a solar pond is using a heat exchanger located inside the LCZ. First, fluid passes through the internal heat exchanger, and then it transmits its thermal energy to the external heat exchanger, shown in Figure 2.14. Expansion tank was placed nearly 2.5 meters above the ground, with a capacity of 1000 liters, and it was composed of a linear low-density polyethylene with fresh water. It charged the heat extraction system and permitted expansion throughout the process. Water circulation through the heat exchanger was provided by a pump. In addition, the heat exchanger was designed to produce a heat output of 60 kW. This method was used at Pyramid Hill SGSP in Australia (Leblanc et al., 2011).

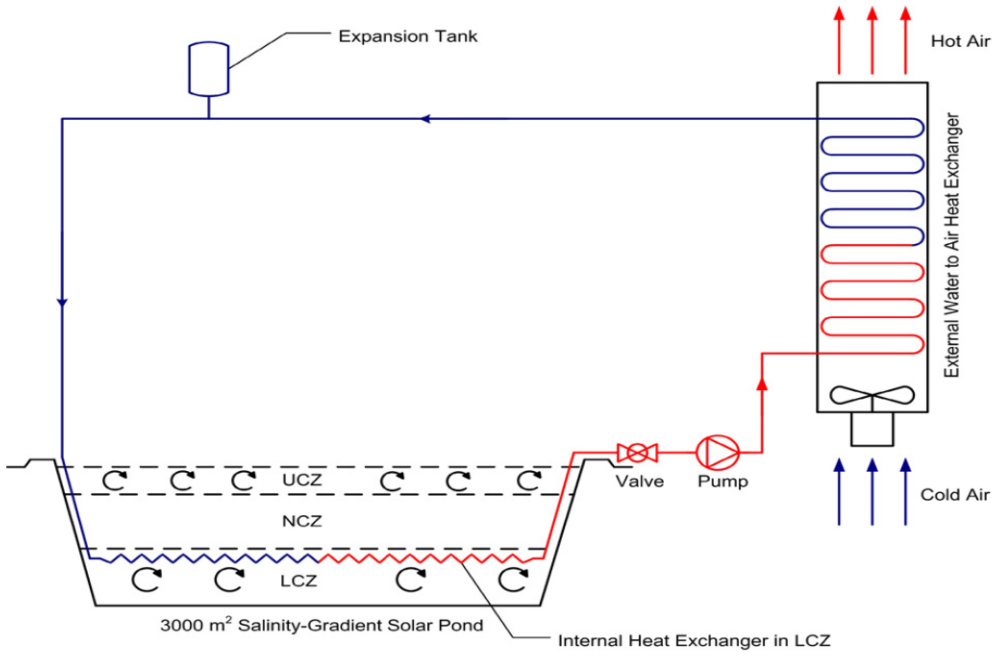

Figure 2.14. Heat extraction method by using an in-pond heat exchanger as an example of Pyramid Hill Solar Pond (Leblanc et al., 2011).

Employing an external heat exchanger in LCZ is another method of heat extraction which was applied in El Paso SGSP in USA. In this method, extraction diffuser is used to take hot brine from the top of the lower layer, LCZ, and then pumped through an external heat exchanger. It then returns through the bottom of the lower layer at a low temperature by using a return diffuser, which is shown in Figure 2.15. Using this method, speed of brine, which needs to be pumped, should be adjusted properly to avoid erosion in NCZ. It is known that convection and salt diffusion can create erosion and it is resulted in the boundary motion, which decreases the thickness of the gradient zone. Therefore, surface washing on the UCZ and regular brine addition to the bottom layer are essential to prevent erosion. Moreover, it is possible to move external diffuser, where the highest temperature in LCZ is obtained. As mentioned before, cooled brine returns to the bottom of LCZ, which decreases the loss caused by ground (Leblanc et al., 2011).

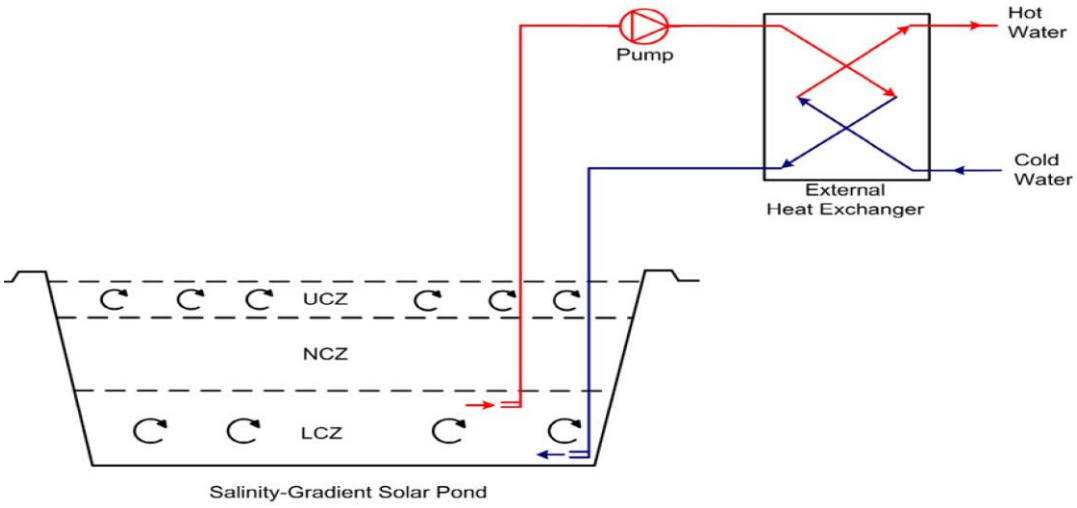

Figure 2.15. Schematic of External heat exchanger method used in El Paso SGSP (Leblanc et al., 2011).

Therefore, two fundamental methods providing heat extraction from the bottom layer of the SGSP were investigated by Leblanc et al. in 2011. First method is the circulation of hot brine taken from LCZ through an external heat exchanger which was used in El Paso solar pond. Circulating working fluid for the closed cycle is another method which was applied in Pyramid Hill solar pond.

Singh et al. (2011) investigated the combination of thermosyphons and thermoelectric cells to generate electricity in a passive way since both devices are micro scale moving parts. It is known that large-scale solar ponds can produce electricity effectively like the example of a conducted project in Israel, which uses a Rankine Cycle and produces 5 MW electricity. Small-scale solar ponds can only meet the electricity demands such as between 2 and 5 kWh/day for small houses.

Converting thermal energy to power is the main difficulty. For example, heat engines have a complex structure and their cost is not cheap. Moreover, electricity conversion efficiency of thermoelectric cells, TECs, is not high. For example, nearly 2% efficiency is obtained when ΔT is equal to 50°C, whereas their maximum Carnot efficiency reaches only between 10% and 20% at the same ΔT. TECs can be used in small size applications including small-scale solar ponds since they are not only small but also a simple tool to convert energy. Furthermore, recent studies showed that their

efficiency level had been increased due to the enhancements in semiconductor materials that are used in these cells (Singh et al., 2011).

Thermosyphons are effective devices that are used for heat transfer by means of latent heat of a working fluid, which is water. Transferring huge amounts of heat can be obtained if the latent heat of vaporization is high enough. Additionally, converting temperature variances to electrical potential while producing power can be maintained by thermoelectric cells. There are many factors that impact generated power such as the difference in temperature between the hot side of thermoelectric cell and low temperature in a heat sink, semiconductor materials like n or p-type, as well as external load resistance (Singh et al., 2011).

By using gravity assisted thermosyphons, transformation of heat is provided by starting from the bottom of the pond to the hot region of the thermoelectric cells. In the evaporator section, evaporation of the working fluid is observed continuously, obtaining vapor then moves upwards to the condenser section of the thermosyphon, where the condensation of vapor occurs and then releases latent heat and travels through the cells. The cold side of the thermoelectric cell is contacted with the cold environment of the top layer of the solar pond. After that, due to the gravitational force, condensed vapor moves down. Therefore, thermoelectric cell, having two sides is obtained at varying temperatures, producing an electrical potential, as shown in Figure 2.16. Produced electric energy can be stored in batteries, which might be used during high demand.

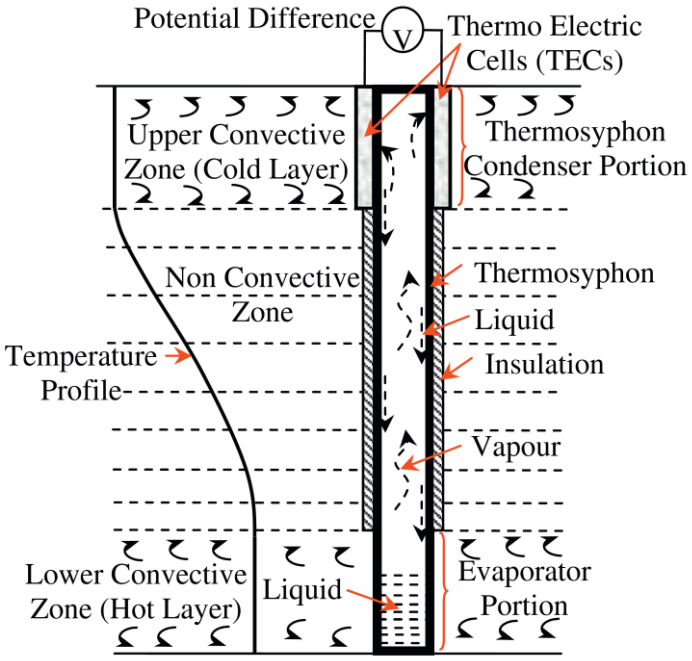

Figure 2.16. Combination of thermosyphon and thermoelectric cells to produce electric power from SGSP (Singh et al., 2011).

According to laboratory results, output power production obtained by TTM, thermosyphon thermoelectric module, increases with rising temperature difference maintained by thermoelectric cells. For example, the maximum output power is maintained at 90°C, which is the evaporator surface temperature, when the maximum temperature difference, 27°C, is obtained across 16 TECs. Therefore, decreasing temperature difference causes maintaining less amount of power output, which can be seen in Figure 2.17.

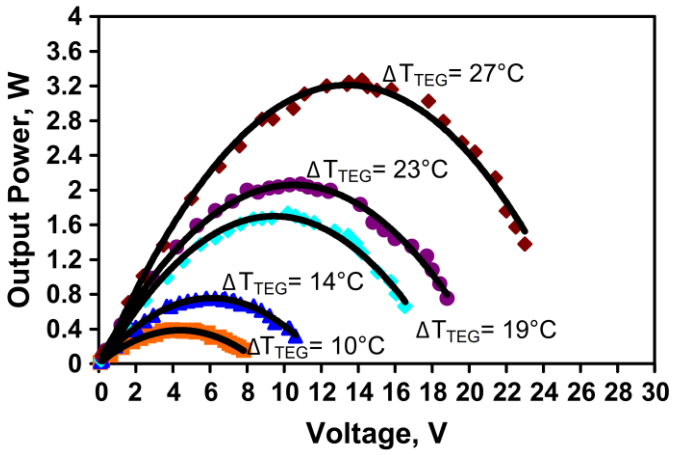

Figure 2.17. Produced power versus voltage graph at different temperatures across the thermoelectric cells (Singh et al., 2011).

Furthermore, based on test results, parabolic curve shape is maintained for the output power, as shown in Figure 2.18. By looking at this figure, at approximately 14 voltages and a current of 0.2 ampere gives almost 3.2 output power (W), which is the maximum outcome.

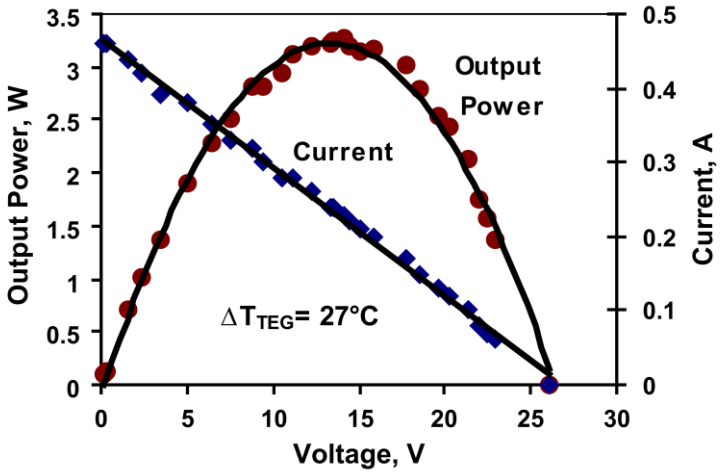

Figure 2.18. Output power at different voltage and current values (Singh et al., 2011).

Laboratory scale model including the combination of thermosyphon and thermoelectric cells was investigated in the SGSP at different temperature differences (Singh et al., 2011). Results of this research showed that a system composed of TTM could be used to generate power for a small size salt gradient solar pond. Furthermore, this system can continue to supply useful power output even if at nights and when the cloudiness index is high due to the thermal storage on the SGSP, which is a significant advantage (Singh et al., 2011).

CHAPTER 3
METHODOLOGY FOR EXPERIMENTAL PART

This chapter provides detailed information about the experimental methodologies applied in this study.

A prototype of a solar pond was constructed at the Middle East Technical University Northern Cyprus Campus (METU NCC) during a previous study. However, the pond was repaired, reconfigured and refilled during the current investigation. The solar pond used, was 61 cm in diameter and 55 cm in height. The pond was placed on a polyurethane insulator foam, having 1.2 cm of thickness, to minimize the heat loss that might occur from the ground and side walls. This small-scale solar pond was equipped with both three sampling valves and three inlet ports, located at different heights of the pond. Three sampling valves were used to take samples from each layer to measure the salt concentrations, whereas three inlet ports were used to add proper amounts of salt solution to each layer.

Before each experiment, a calibration curve was developed using a conductivity meter (Multi 3420) to properly measure salt concentrations of solar pond layers before and during the experiments. The calibration curve, Figure 3.1, was obtained by dissolving different amounts of salt in 200 ml water. After dissolving specified amounts of salt in water, precipitation was observed, and the conductivity level reached a constant value.

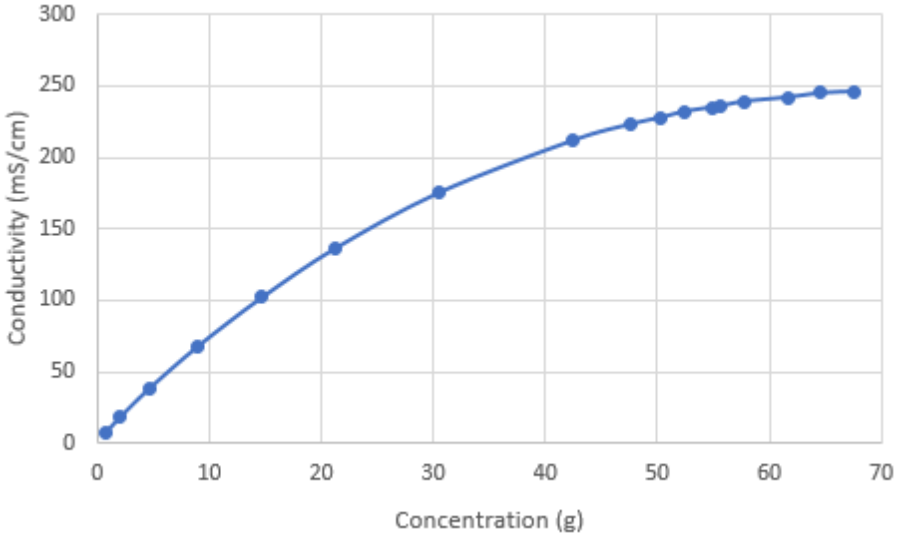

Figure 3.1. Conductivity versus concentration plot for the experimental process.

After getting the calibration curve, the pond was filled with a solution of water and NaCl due to its availability and low cost. The bottom layer had the highest amount of salt; assuming its concentration was equal to C. The volume of LCZ was 75 L and approximately 21 kg of NaCl was used to fill LCZ. Moreover, additional salt was placed at the bottom of the pond to compensate for the salt diffusion through the upper layers and to make sure that LCZ was always saturated with salt. The gradient layer, which is also known as the non-convective zone, NCZ, comprises of three sublayers and their salt concentration levels decrease with increasing height. Volume of each sublayer is 15 L. Starting from the bottom sublayer; salt concentrations of these layers were prepared as 3C/4, C/2 and C/4, respectively. The total amount of NaCl used in NCZ was approximately 6.3 kg. The surface layer, UCZ, contained only fresh water without any brine and the volume of this layer was 15 L. To control the salt concentrations, 10 ml of samples from each layer were taken through the attached valves. After that, the conductivity of samples was measured by a conductivity meter. Using samples that were taken from valves were added to both NCZ and LCZ for compensating sampling losses.

Furthermore, at the beginning, 6 thermometers including 2 for each layer were used to measure layer temperatures. Obtained average temperatures for each layer that were measured from thermometers recorded twice a day at 12.30 pm and 17.30 pm. For example, only 2 thermometers, placed at the middle of NCZ, were used to measure average NCZ temperature. As mentioned before, it consists of three sublayers and temperature estimation of each sublayer could not possible by using these thermometers.

As a result, to obtain more accurate and higher time resolution data within days, thermocouples were decided to be used. K-type thermocouples, which is one of the most common types of thermocouples, were used in this experiment since they are reliable, cheap and have a wide temperature range.

They were used at different depths to record the temperature distributions during the experimentation on between April and June in 2017, as indicated in the Figure 3.2. First, different amounts of water (10, 15 and 20 liters) were added to the empty pond to measure the heights of each layer and the results were found as 3.5, 5.5 and 7.5 cm respectively. Using this method, the heights of LCZ, NCZ, and UCZ were estimated and the location of the thermocouples inside the pond was determined based on these heights. Figure 3.2 illustrates the positions of the thermocouples used to measure the temperature distribution in the solar pond. For instance, LCZ had 75 liters of salty water and the average height was determined as nearly 28 cm, and three thermocouples were placed at 8, 16 and 24 cm heights of the pond to monitor the temperature distributions in LCZ. Furthermore, 12 of these thermocouples were located at different heights, and rest of them, numbered as 1, 2 and 3, were placed at 8 cm higher from the bottom of the pond to obtain radial temperature distribution in LCZ. Thermocouple number 7 (at 32 cm from the bottom of the pond) represents the bottom sublayer of the NCZ whose average height was found as 32.75 cm, whereas thermocouples numbered 8, 9 and 10 were in the middle sublayer of the NCZ and their heights were 35, 37 and 39 cm, respectively. Remaining sublayer closer to the UCZ includes thermocouples 11 and 12, which were positioned at the heights of 41 and 42 cm, respectively. Finally, at the top of the pond in UCZ, thermocouples numbered as 13 and 14 were placed at 46 and 47 cm, as indicated in Figure 3.2.

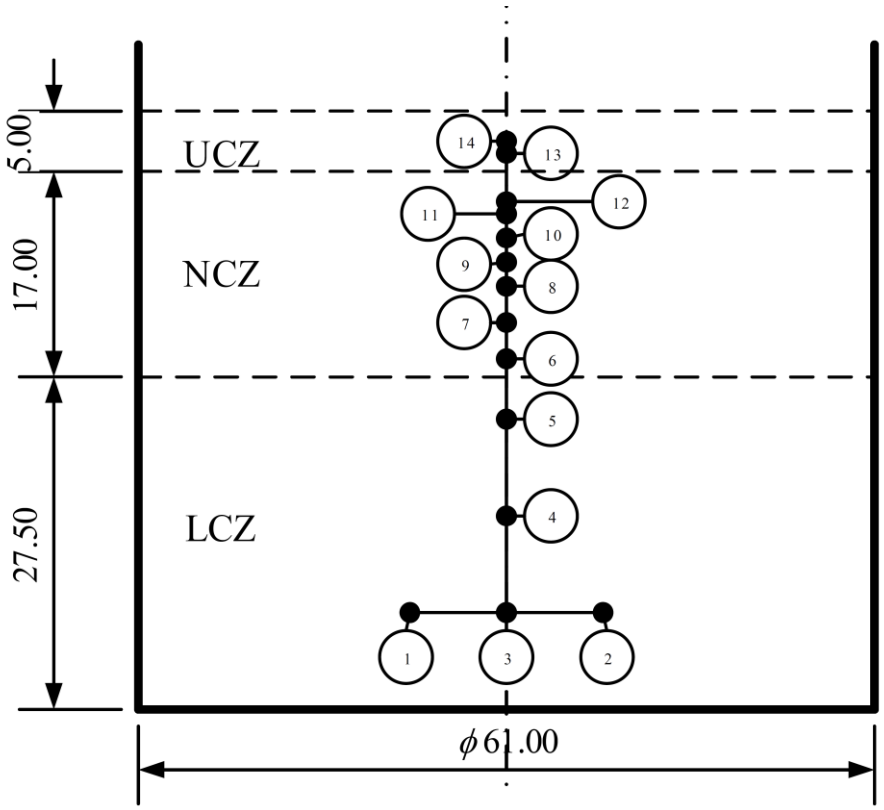

Figure 3.2. Prototype of small-scale solar pond at METU NCC, including the heights of each layer and the positions of the thermocouples (Taylan et al., 2017).

To estimate the temperature of each layer, another calibration curve including temperature and voltage readings were created by using a multimeter, as shown in Figure 3.3. Multimeter is a device used to measure the level of voltage, resistance, and current. An equation was obtained to calculate the temperature using the voltage differences.

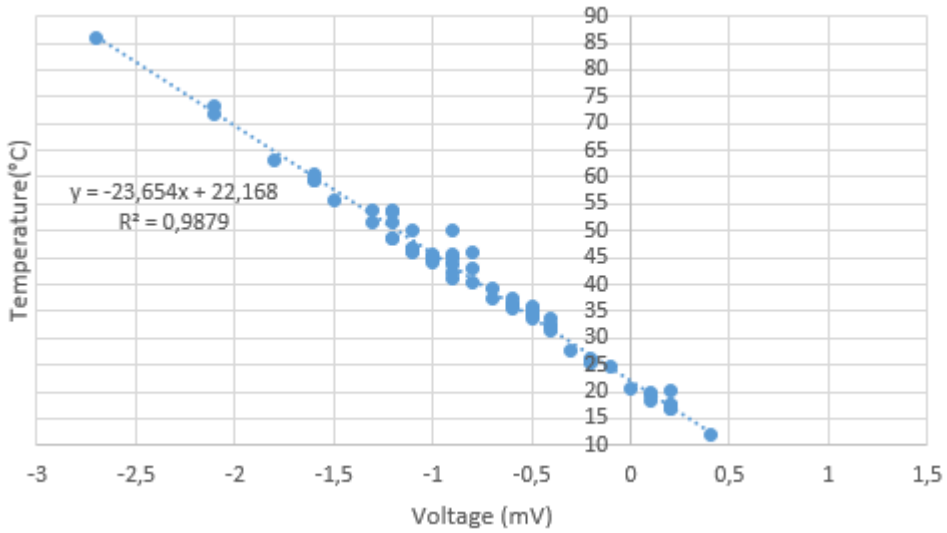

Figure 3.3. Calibration curve prepared for the thermocouples.

Average voltage readings obtained from the thermocouples were recorded at 10-minute intervals using a data logger (Campbell Scientific CR800 and AM16/32B Multiplexer). Not only for monitoring but also processing the output data, network interface an adapter (Campbell Scientific NL201) was connected to a computer system, and data collection was supplied during the experiment.

Solar insolation, wind speed as well as ambient temperature were measured to evaluate the performance of the SGSP. The solar radiation incident on the horizontal surface was recorded at an interval of 10 minutes by using a pyranometer (Kipp and Zonen CMP22), whereas direct normal insolation was measured with a pyrheliometer (Kipp and Zonen CHP1). Both devices were connected to a sun tracker (Kipp and Zonen Solys 2). By using a sensor named Galltec KPC 1/5, ambient temperature and relative humidity recorded. Additionally, wind speed data was measured using an anemometer.

Surface washing is required to prevent the accumulation of diffused salt and for compensating evaporation loss during the experiments. This is an important step to maintain the salt concentrations which was adjusted at the beginning. It is understood that from the bottom layer to upper layer, diffusion of salt is observed; thus, surface washing which means refreshing the surface layer is essential for this experimentation. As a result, surface washing was done every week but starting from summer, it was done every 3 days during the experimentation. For the washing process, first, UCZ

water was emptied, then, the initial volume of UCZ, 15 liters, was added very slowly to prevent mixing with other layers. Hence, surface washing provided stable UCZ concentration.

In this study, about 2 months of data between April and June in 2017 was used to investigate the experimental results, because after using thermocouples, the collection of datum was provided every ten minutes; thus, time resolution of this study was high enough for examination.

3.1 Heat Loss Calculation

It is known that heat transfer by convection at a surface is measured by Nusselt number, Nu, and it is a function of Reynolds number (Re) and Prandtl number (Pr), which can be seen in Equation (2). With the knowledge of Nu, convection coefficient, h, can be determined (Bergman et al., 2011).

$$\overline{Nu} = f(Re_L, Pr) = \frac{\bar{h}L}{k_f} \tag{2}$$

For convection, total heat transfer rate, which is also known as Newton's law of cooling, can be calculated as:

$$q = \bar{h}\, A_s(T_s - T_\infty) \tag{3}$$

Furthermore, wind speed distribution has a significant effect on the convective heat and mass transfer so that nature of the flow on the UCZ, which includes laminar and turbulent flow, should be investigated to understand the heat convective losses.

Flow conditions on the surface of the pond should be investigated by using Reynolds number, which can be calculated by using Equation (5), assuming the surface of the pond is a flat plate and there is an external flow on the surface layer of the pond, as well as surface layer of the pond is isothermal (Bergman et al., 2011). For instance, the range of Reynold number for the turbulent flow is between $5x10^5$, which is the critical Reynolds number, and 10^8, shown in Equation (4), as well as it is defined as in Equation (5).

$$Re_{x,c} \leq Re_x \leq 10^8 \tag{4}$$

$$Re = \frac{\rho V d_p}{\mu} \tag{5}$$

where V shows the velocity of wind, d_p represents the diameter of the pond, ρ is the density of the fluid, and μ is the viscosity of the fluid. Fluid is the ambient air and its properties were evaluated at 300 K. According to calculations, flow type was found as laminar under all observed conditions. After that, Nusselt number for the laminar flow conditions over the surface can be calculated by using Equation (6) and assuming the surface of the pond is a flat plate and there is an external flow on the surface layer of the pond, as well as surface layer of the pond is isothermal.

$$\overline{Nu}_x = \frac{\overline{h_x}(x)D}{k} = 0.664\, Re_x^{1/2} Pr^{1/3} \qquad Pr \geq 0.6 \tag{6}$$

where Pr and k, which are the Prandtl number and the constant thermal conductivity of a fluid, respectively, at 300 K are given as 0.707 and 0.0263 W/m·K, respectively. Additionally, D is the diameter of the pond, and for each wind speed value, h was calculated separately. Using Equation (3), the relation between heat transfer rate and the convective heat transfer coefficient can be examined to understand the effect of convective losses on UCZ.

3.2 Pond Efficiency

Efficiency of the solar pond is calculated using,

$$\eta = \frac{Q}{I\,A} \tag{7}$$

where I is the daily total GHI, A is the area of the solar pond, and Q is the quantity of heat can be calculated as,

$$Q = m_{LCZ}\, c_p\, \Delta T \tag{8}$$

where m_{LCZ}, c_p are the mass and the specific heat of the lower convective zone, respectively. Additionally, ΔT shows the temperature difference between the lower convective zone and ambient air.

3.3 Uncertainty Calculation

It is known that there is always a boundary of suspicion for every measurement and uncertainty can be defined as a quantification of the doubt that is related to the results. Therefore, it is very crucial to define the sources of uncertainty which are used in the measurements (Bell, 1999).

Uncertainty can be found by taking the square root of the total uncertainties of measurements and calculated by using Equation (9).

$$Uncertainty = \sqrt{a^2 + b^2 + c^2 + \cdots etc.} \quad (9)$$

where a, b and c are the uncertainty of the K-type thermocouple, platinum resistance thermometer (Pt-100), and datalogger, respectively.

For example, the uncertainty in data acquisition and power supply are assumed to be neglected because they are very small. Additionally, tolerance level of K-type thermocouple changes about $\pm$3ºC between the temperature intervals of 0ºC to 400ºC (Bentlay, 1984). Furthermore, accuracy for PT-100 can be found as 0.06 ºC based on the datasheet of the material.

Therefore, combined uncertainty of these materials is found as about $\pm$3ºC, which is used to validate of the numerical results with the results of experiments in Section 6.1.

CHAPTER 4
RESULTS AND DISCUSSION OF EXPERIMENTAL PART

Using distribution of temperature and the weather conditions, experimental evaluations of the salt gradient solar pond (SGSP) was conducted. According to the experimental data, some of the important results are given in this chapter. Daily average values of the temperatures of LCZ, UCZ, and ambient temperature, wind speed as well as global horizontal insolation as daily sum between the period of 18th April and 23rd of May can be seen in Figure 4.1. It is known that obtaining higher LCZ temperature is important to store solar energy, which mainly depends on both ambient temperature and incoming solar radiation. Based on obtained results, it can be seen that the temperature of the lower convective zone is higher than both ambient temperature and UCZ temperature since incoming solar radiation is mostly trapped in this area. This observation proves that solar insolation can reach the bottom layer of the pond. Similarly, higher LCZ temperature is obtained when the incoming solar radiation is high, which is illustrated in Figure 4.1. For example, the first peak point on the GHI was obtained between 18th and 19th April. Approximately 7.7 kWh/m^2 of daily total global horizontal insolation was recorded on 19th April, which resulted in the increase in temperature of LCZ from 30°C to 34°C. Additionally, during this period, one of the greatest values of GHI was recorded on 7th May, which was about 8 kWh/m^2 and temperature of LCZ reached up to 38°C. Therefore, the temperature of LCZ and GHI values follow a similar pattern.

Moreover, it is generally expected that the temperature of surface layer decreases with increasing wind speeds, which might result in the decreasing of the LCZ temperature. For instance, the highest average wind speed, which was 12 m/s, and one of the minimum ambient temperatures, about 16°C, were observed on 23rd April. However, on this day, LCZ temperature did not follow a decreasing path, on the contrary, it reached one of its highest values, about 38°C. This might be because of the increasing incoming solar insolation (about 8 kWh/m^2) that reaches to the area of the pond. Hence, the wind speed does not have a profound effect on the LCZ temperature. Any changes of wind speed might be accompanied by changes in GHI or ambient temperature that collectively impact the pond temperatures.

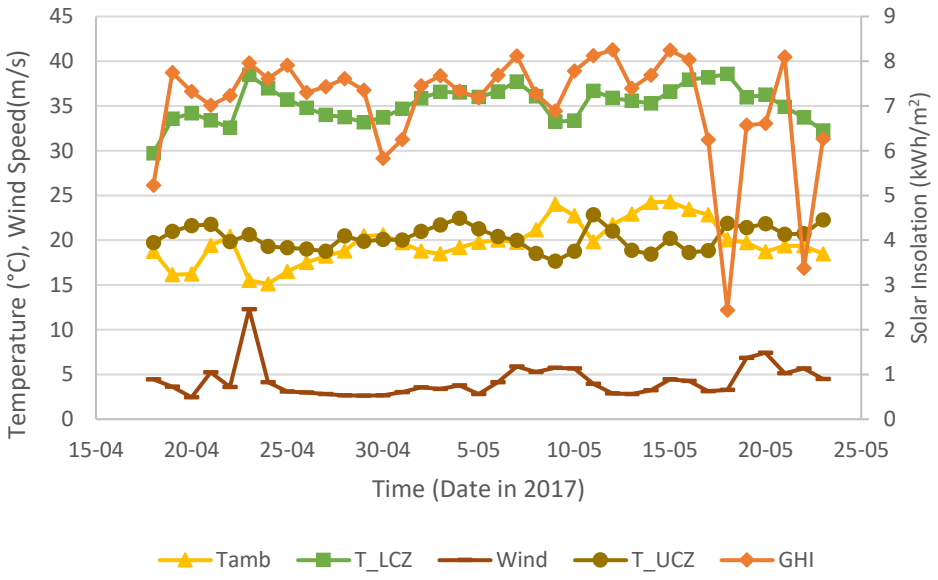

Figure 4.1. Variations on the daily average temperatures including LCZ, UCZ and ambient, wind speed and daily total solar insolation on between April 18, and May 23.

Besides, it was observed at some points in Figure 4.1, while ambient temperature increases, the bottom layer and surface layer temperatures decrease. Ambient temperature and layer temperatures including UCZ and LCZ generally followed each other in a contradictory way in this period, which was one of the most interesting results of this experiment. When considering the temperature of UCZ, it should have increased with increasing ambient temperature and vice versa. Higher convective loss from the SGSP might be the significant reason for this adverseness. To understand its effects, the relationship between temperature gradient and convective heat transfer should be investigated, which was explained in Section 3.1.

According to the results, heat transfer rate was found to be negative at some points, which proves that convective heat loss occurs from UCZ to the atmosphere. For instance, the ambient temperature was recorded as 24ºC on 9th of May, whereas the temperature of UCZ was 17ºC. Based on calculations, one of the greatest values of convective heat transfer coefficient, h, was found as about 12 W/m^2·K, which directly affects the heat transfer rate per unit area, q, found as 85.3 W/m^2. Largely as a result of these significant heat losses, UCZ temperature was lower than expected. On this day, one of the highest values of wind speed was recorded as about 6 m/s. It can be observed that wind speed increased from 3 m/s to 6 m/s on 7th of May, and stayed about 6 m/s until 10th of May. Additionally, GHI followed a decreasing pattern during

this period, which might be resulted in decreasing UCZ temperature. However, the temperature of UCZ and ambient temperatures were found to be approximately the same on 29th April, which was about 19ºC. On this day, convective heat transfer coefficient, h, was found as about 8 W/m^{2}·K. As mentioned before, lower h results in lower heat transfer rate; thus, about 13 W/m^{2} convective heat loss through the outside was observed. This explains that the temperature of the surface layer and ambient temperatures were close to each other.

Another example can be seen on 23rd of April, where UCZ temperature (about 20ºC) was higher than the ambient temperature (about 15ºC). The daily average wind speed was high (12 m/s) on this day but GHI showed an increasing trend from 7 to 8 kWh/m^{2} based on the day before, which has resulted in obtaining a higher UCZ temperature. The rate of the GHI influence on the temperature gradient of the pond was sufficiently high to reach a temperature at UCZ higher than ambient temperature, then, the negative heat loss occurred such that the UCZ temperature reduces and becomes equal to the ambient temperature.

As a result, GHI has a more significant impact on controlling the temperature of the layers than ambient temperature and wind speed. It directly controls the temperature trend of LCZ. It also controls the UCZ temperature, but due to the presence of convective heat transfer and changes in ambient temperature, changes in UCZ temperature is not fully similar to the GHI variations. Therefore, a compromise exists between the effect of GHI and ambient temperature of UCZ temperature. Furthermore, wind speed is not really a major contributor. However, its effect will be embedded in the Reynolds number, representing the heat transfer loss.

To prevent these convective losses, some solutions should be suggested. It is known that evaporation is another important reason for heat loss from surface layer to atmosphere; thus, to prevent this, Satish (2015) suggested covering the SGSP with transparent materials, which is resulted in not only reducing heat loss but also developing the performance of the pond. Absorbing the incoming solar insolation and preventing heat loss because of the evaporation rate are the main purposes of covering the surface with transparent materials such as film-coated glass sheet or plastic transparent black (Patel et al., 2015). Additionally, reflectors such as a mirror or stainless steel sheet can be used to catch reflection during the day. However, the size

of the reflectors is important. For instance, Patel et al. (2015) suggested that their size should not pass the 1/3 diameter in height to catch the reflection. Therefore, these options can be some basic solutions for the heat loss from the SGSP.

Figure 4.2 shows the data including temperatures, wind speed and solar insolation on an arbitrarily chosen day (19th April), which was collected every ten minutes. Evaluations of results were similar to variations on the daily average temperatures including LCZ, UCZ, and ambient, wind speed and solar insolation on between 18 April and 25 May. UCZ and LCZ temperatures followed a similar pattern. By looking at Figure 4.2, GHI can be observed only between 6 am and nearly 8 pm, in other words, between the period of sunrise and sunset. Moreover, its values are high around solar noon from 12 pm to 2 pm, varying from 950 W/m^2 to 978 W/m^2. At this period, ambient temperature also reached its highest value, which was about 21ºC. Moreover, it was seen that after 12 pm, both LCZ and UCZ temperature started to increase. Hence, higher solar insolation causes higher LCZ temperature, which proves solar insolation can reach to the bottom layers. Wind speed was generally around 6 m/s at this period, and change in the ambient temperature did not affect LCZ temperature significantly. This result might be because of the high heat capacity of the lower layer.

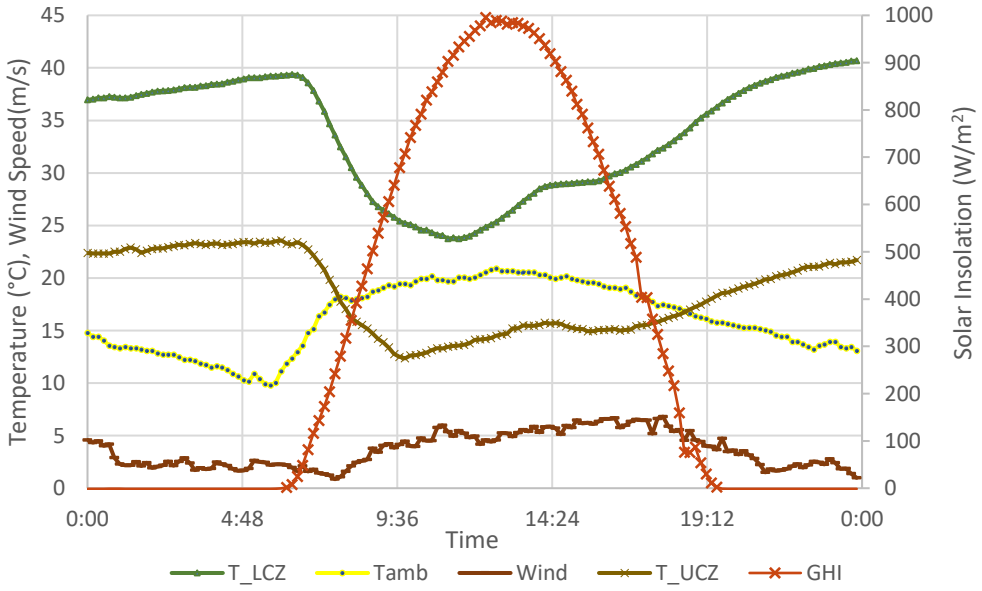

Figure 4.2. Variations on the average temperatures including LCZ, UCZ and ambient, wind speed and solar insolation on 19th April.

Other results obtained from the experimental part are illustrated in Figure 4.3. This figure shows the distribution of wind speed, solar insolation, temperature differences between LCZ and UCZ, as well as temperature differences between LCZ and ambient air for the period from April 18 to May 31, 2017. The evaluation of the results of this figure is nearly the same as Figure 4.1. The relation between the ambient conditions and the temperature differences between the layers is the main objective of this figure.

Additionally, detailed information including GHI, ambient temperature, wind speed and the temperature differences between the LCZ and UCZ of the examined days can be seen in Table 4.1.

Table 4.1. Parameter information related to Figure 4.3

Day	GHI (kWh/m^2)	T_{amb} (°C)	U_w (m/s)	T_{LCZ}-T_{UCZ} (°C)
22.04.2017	7.23	20.4	3.5	12.7
23.04.2017	7.96	16.5	12.3	17.8
24.04.2017	7.61	15.1	4.1	17.6
21.05.2017	8.10	19.4	5.2	14.2
22.05.2017	3.38	19.4	6.0	12.9

For instance, wind speed was recorded as about 4 m/s on 22nd of April, whereas approximately 12 m/s of wind speed was observed on 23rd of April. Between 22nd and 23rd of April, a 4°C decrease in ambient temperature was observed.

As a result of an increase in wind speed, an increase in temperature differences between the LCZ and UCZ is expected. The reason for this expectation is that, at higher wind speeds, UCZ temperature might decrease due to the increasing water evaporation rate; thus, the temperature differences between the LCZ and UCZ increases. Similarly, when the ambient temperature decreases, again it is expected to decrease UCZ temperature; thus, temperature gradient increases. Furthermore, based on recorded data; GHI increased from 7.23 to 7.96 kWh/m^2 and similarly DNI changed from 5.93 to 8.95 kWh/m^2 between these days, which directly resulted in increasing LCZ

temperature from 32°C to 38°C. The main reason for obtaining about 5°C of T_{LCZ}-T_{UCZ} increase was increasing LCZ temperature, since, between 22nd and 23rd of April, UCZ temperatures were similar to each other, which were recorded as about 20°C.

However, the next day, on 24th of April, when the wind speed showed a sharp decrease to nearly 4 m/s, nearly the same temperature differences were maintained, although daily total GHI showed a small decrease from 7.96 to 7.61 kWh/m^2. Moreover, average LCZ temperatures on these two days were recorded as 38ºC and 36ºC, respectively. The high heat capacity of the LCZ might be one of the reasons for obtaining nearly similar temperature gradient. Having a close ambient temperature and GHI values on these days might be the other reason for maintaining the nearly same temperature gradient. Additionally, it can be understood that wind speed did not have a profound effect on the temperature gradient.

Moreover, there was nearly the same amount of wind speed and ambient temperatures on both the 21st of May and 22nd of May, which can be seen in Table 4.1. However, the daily total solar insolation decreased from about 8.1 to 3.4 kWh/m^2; thus; temperature differences followed a decreasing path.

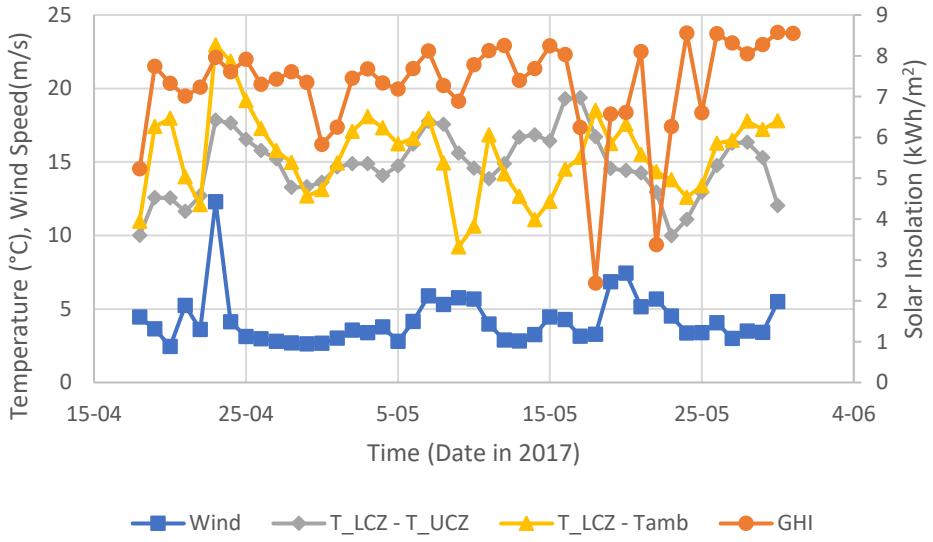

Figure 4.3. Variations on the temperature differences between LCZ and UCZ, LCZ and ambient temperature, wind speed and global horizontal insolation.

Moreover, to understand the temperature distribution in the SGSP at different heights, Figure 4.4 and Figure 4.5 were obtained at different times on a randomly chosen day. Although they are randomly chosen, they are representative temperature distributions.

Besides, these figures show the place of eleven thermocouples (in heights) to evaluate the temperature distribution for each layer. Thermocouples at the heights of 8, 16, and 24 cm fall within the LCZ layer, the one at 32 cm is in the NCZ_3, the ones at 35, 37 and 39 cm are in the NCZ_2, the ones at 41 and 42 cm show the NCZ_1 temperature, and finally, the ones at 46 and 47 cm represent the UCZ temperature.

There were slight temperature variations in both UCZ and LCZ, while more linear temperature distribution occurred in the NCZ. Both figures have linear temperature profiles for the NCZ. Temperature increases with height in NCZ as expected, and the temperature gradients can be easily seen at between the heights of 32 cm and 42 cm. Besides, NCZ behaves as a thermal barrier to prevent the heat diffusion from LCZ to UCZ. Furthermore, LCZ temperatures have the highest values as expected. Moreover, it can be observed that temperatures obtained at 7 am were higher than the values of 5.30 pm. This shows that even if there is no or low solar radiation, solar pond continues to keep its temperature.

Therefore, the salt gradient solar pond can be used as a thermal storage system by looking at these temperature distributions that are shown in Figure 4.4 and Figure 4.5, when the temperature difference between the LCZ and surroundings is about 22ºC and 13ºC, respectively.

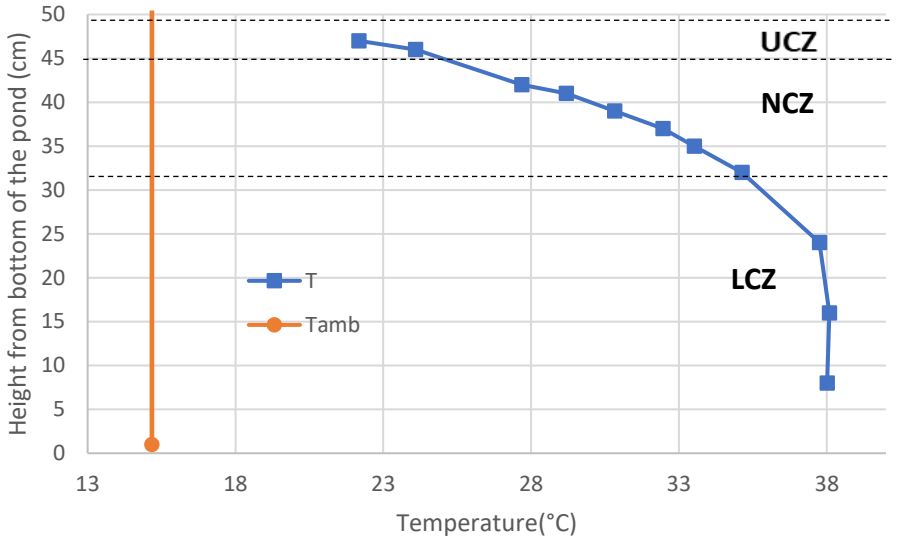

Figure 4.4. Temperature distribution in SGSP and ambient temperature at 7 am on April 19, 2017.

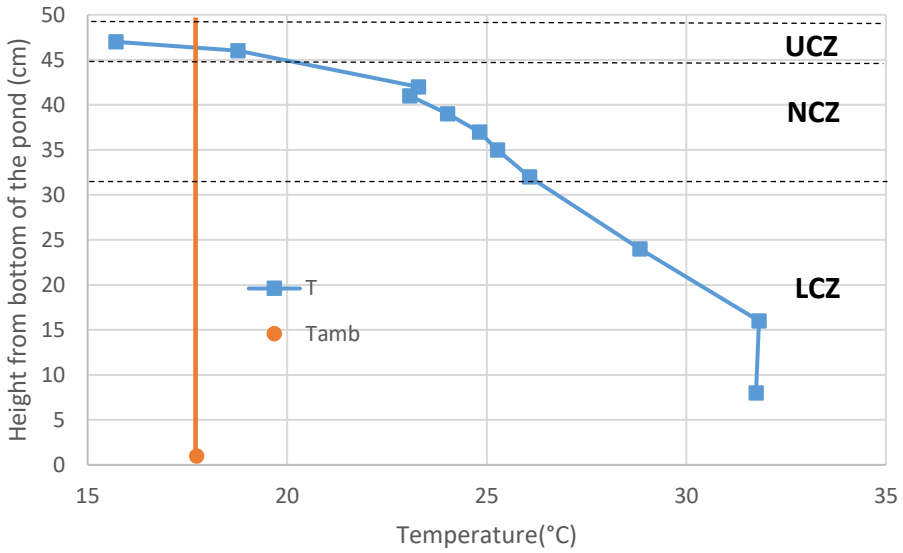

Figure 4.5. Temperature distribution in SGSP and ambient temperature at 5:30 pm on April 19, 2017.

Finally, the daily efficiency of the pond was calculated on between 18th April and 13th June. Calculated daily pond efficiencies varied from 29% to 90% according to the Equation (7) and (8). The minimum efficiency was calculated to be 29% on 8th June whereas the maximum efficiency was calculated 90% on 23rd April.

On both days, similar daily sum of GHI values were recorded, about 8 kWh/m^2. However, calculated heat values, and temperature differences between the lower layer and ambient temperatures varied. For example, calculated heat values were found as 7700 kJ on 23rd of April, whereas about 2500 kJ was found on 8th June. Similarly,

small temperature differences in the lower layer were found, these were recorded as 38ºC on 23rd April and 33ºC on 8th June, but temperature gradient was higher on 8th June than 23rd April, since ambient temperature (25ºC) was higher than the temperature of 23rd April (15ºC).

Depending on the definition, efficiency calculations may change. For example, based on research, collected annual efficiencies on small ponds was found to be 15% (Valderrama et al., 2016). Similarly, about 25% of pond efficiency, mostly depending on depth, hygiene as well as temperature of the pond, was calculated for a 100 cm depth of a SGSP (Tabor et al., 1965).

CHAPTER 5
METHODOLOGY FOR NUMERICAL PART

This chapter provides detailed information about the numerical methodologies applied in this study.

There were some difficulties in the experimental part. For example, thermocouples are very sensitive and might give errors; thus, it was required to check them constantly. Additionally, there were coupled effect of incoming solar insolation, wind speed and ambient temperature on the layer temperatures. Therefore, it was very difficult to investigate each effect individually. Furthermore, there was only one small-scale pond for using experimentation; thus, it was impossible to change the diameter or thickness of the layers for the investigation. As a result, in the numerical part, COMSOL Multiphysics, which is a software program based on finite element methods, was used since it provides an environment in which difficulties are minimized. Additionally, it provides both a complete and integrated environment to create both modeling and simulation (Multiphysics, COMSOL, 1998). In this thesis, modeling in COMSOL was done to investigate the following three major aspects.

Firstly, collected experimental data, which includes ambient temperature, relative humidity, wind speed, layer temperatures, and insolation, were used as inputs to the program, and transient simulations were performed for both 600 and 7200 seconds. After that, temperatures of the layers that were computed by the simulation program were compared to the results of the experiments, which was required for the validation of the modeling. Secondly, the effects of weather including ambient temperature, wind speed, as well as solar insolation on the layer temperatures were examined individually. Finally, the effects of pond geometry such as diameter and layer thicknesses on the layer temperatures was investigated.

At the beginning, the global definitions node, used for describing parameters, variables as well as functions, was created. Parameters are constant scalars, which are defined by users (Multiphysics, COMSOL, 1998). Table 5.1 shows the parameters that were used in the modeling part of this thesis.

Table 5.1. Parameters that were used in COMSOL.

Parameter	**Description**
c0	Initial concentration
dia	Pond inside diameter
H_vap	Heat of vaporization
height	Pond height
height_LCZ	Height of LCZ
height_NCZbottom	Height of bottom layer of NCZ
height_NCZmiddle	Height of middle layer of NCZ
height_NCZtop	Height of top layer of NCZ
height_UCZ	Height of UCZ
Insolation	Solar insolation (GHI)
M_w	Molar mass of water
rel_hum	Relative humidity of air
rho_w_max	Maximum amount of water
S_LCZ	Salinity of salty water in LCZ
S_NCZbottom	Salinity of salty water in the bottom layer of NCZ
S_NCZtop	Salinity of salty water in the top layer of NCZ
Tair	Ambient temperature
Vwind	Wind speed

Additionally, properties of the model were defined in the part of material contents. For example, salty water for the layers including LCZ and NCZ was defined in this section

as seawater with different salt concentrations. Its material type (nonsolid), appearance (water) and material properties including density, heat capacity at constant pressure, thermal conductivity, and the ratio of specific heats were specified. Furthermore, it was necessary to define some expressions just only for the concentrated layers of the program for obtaining more accurate results such as thermal conductivity, specific heat, and density.

Generally, physical properties of pure water and seawater are close to each other. It is known that seawater is a mixture of salts and water; thus, its salinity must be specified. According to Sharqawy et al. (2010), the difference level between seawater and pure water is specified in the range of 5 to 10%. On the other hand, this small difference might play a huge role in the system design. Consequently, it is very crucial to define its thermo-physical properties properly on the system.

One of the important properties is the thermal conductivity (in W/m K), which is difficult to measure. Increasing amount of salts that are dissolved in water is resulted in decreasing the thermal conductivity. The correlations of seawater thermal conductivity can be seen in Equation (10). This equation is valid for the temperature range from 0ºC to 180ºC, salinity range from 0 to 160 g/kg and has an accuracy of ±3%. For example, for the measurements of thermal conductibility at temperatures higher than 40ºC, this equation is recommended to be used (Sharqawy et al., 2010).

$$log_{10}(k_{sw}) = \log_{10}\left(240 + 0.0002\, S_p\right) + 0.434\left(2.3 - \frac{343.5+0.037S_p}{t+273.25}\right)\left(1 - \frac{t+273.15}{647+0.035S_p}\right)^{0.333} \qquad (10)$$

where k_{sw} is the thermal conductivity of the seawater, S_p is the practical salinity, and t is the Celsius temperature.

Specific heat is the other significant thermo-physical property of seawater that must be defined to the program. Cox et al (1959) claimed that when water bodies having different values of salinity and temperature are mixed uniformly, it is significant to calculate temperature, salinity as well as density of resultant water mass accurately. Besides, information about not only specific heat of seawater but also its variations with temperature and salinity are necessary for these calculations (Cox et al., 1959).

Specific heat, c_{sw}, (in kJ/kg K) correlations of seawater, including validity of temperature between 0ºC and 180ºC, salinity between 0 and 180 g/kg as, can be seen

in Equation (11) with ±0.28 % deviation (Sharqawy et al., 2010). Additionally, variations of the specific heat of seawater that is calculated with Equation (10), at different temperature and salinity range can be investigated by looking at Figure 5.1.

$$c_{sw} = A + BT + CT^2 + DT^3 \tag{11}$$

where,

$$A = 5.328 - 9.76x10^{-2}S_p + 4.04x10^{-4}S_p^2$$

$$B = -6.913x10^{-3} + 7.351x10^{-4}S_p - 3.15x10^{-6}S_p^2$$

$$C = 9.6x10^{-6} + 1.927x10^{-6}S_p + 8.23x10^{-9}S_p^2$$

$$D = 2.5x10^{-9} + 1.666x10^{-9}S_p - 7.125x10^{-12}S_p^2$$

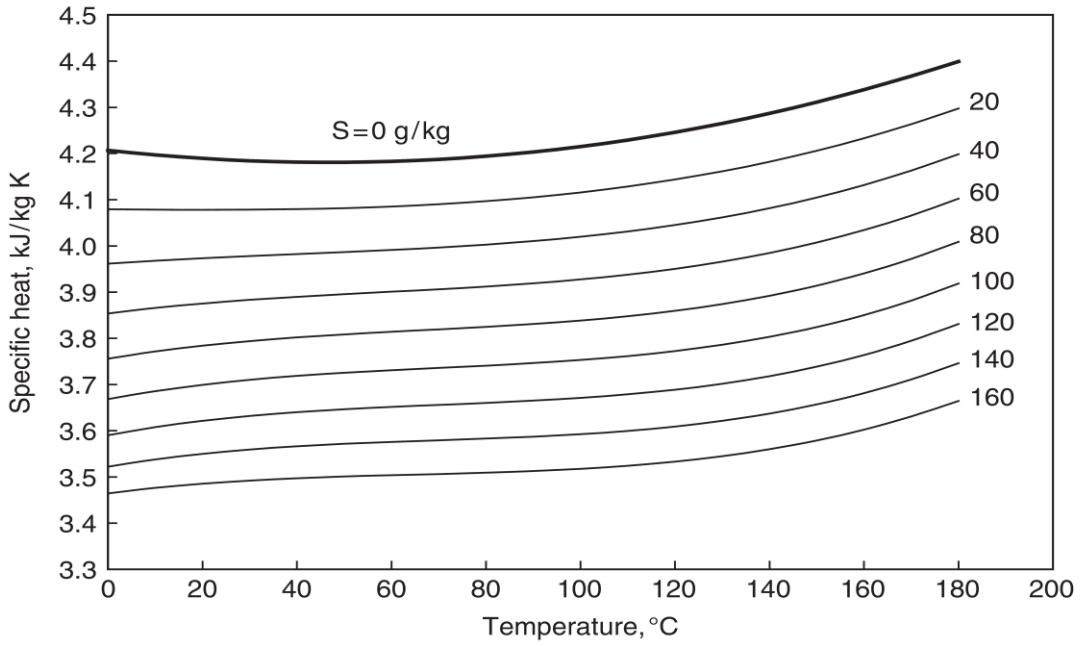

Figure 5.1. Specific heat variations of seawater with different temperature and salinity ranges by using Equation (11) (Sharqawy et al., 2010).

Another important thermo-physical property is the density which should also defined to the program. Seawater density (kg/m^3) at atmospheric pressure, specified at 0.1 MPa, is used for the correlation equation, which can be shown in Equation (12).

$$\rho_{sw} = (a_1 + a_2 t + a_3 t^2 + a_4 t^3 + a_5 t^4) + (b_1 S + b_2 S t + b_3 S t^2 + b_4 S t^3 + b_5 S^2 t^2) \quad (12)$$

where,

$a_1 = 9.999x10^2, a_2 = 2.034x10^{-2}, a_3 = -6.162x10^{*3}, a_4 = 2.261x10^{-5},$

$a_5 = -4.657x10^{-8}, b_1 = 8.020x10^2, b_2 = -2.001, b_3 = 1.667x10^{-2},$

$b_4 = -3.060x10^{-5}, b_5 = -1.613x10^{-5}$

Accuracy of this equation is about ±0.1%, and the range of temperatures and salinities are specified from 0ºC to 180ºC and 0 to 0.16 kg/kg respectively (Sharqawy et al., 2010). Seawater density variations that are measured by using Equation (12) with different temperature and salinity values can be seen in Figure 5.2.

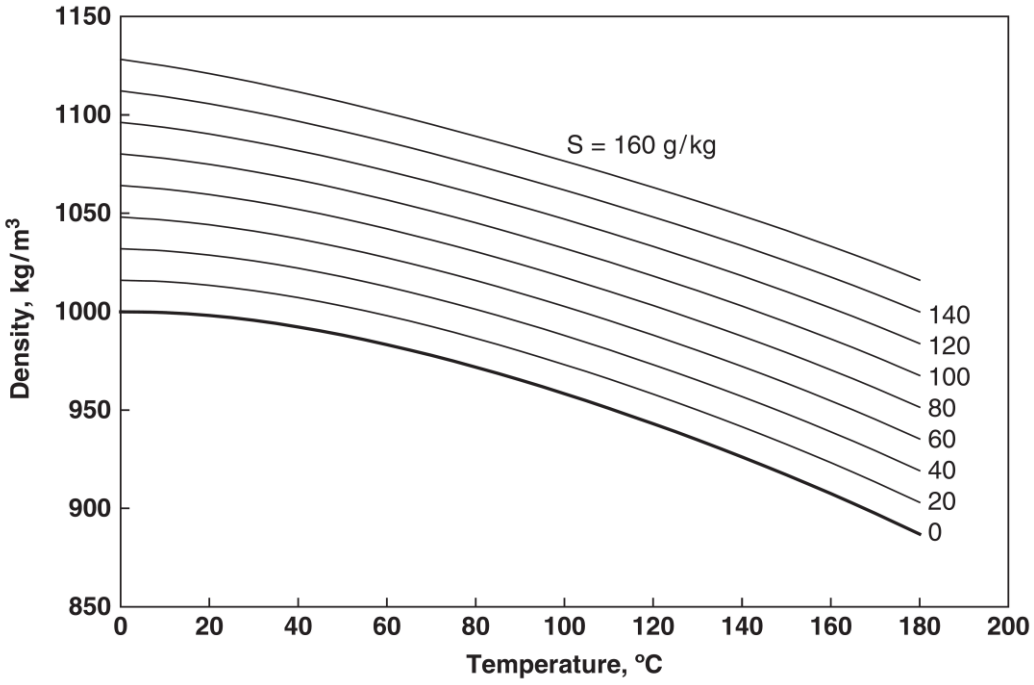

Figure 5.2. Variations of seawater density with temperature and salinity by using equation (12) (Sharqawy et al., 2010).

Furthermore, component definition was also required for the COMSOL. For instance, air, water, and insulation properties were defined in the model. Additionally, geometry of pond, which contains object type, size, and shape such as radius and height, position as well as axis type, was presented. Figure 5.3 shows the general view of the solar pond that was created on COMSOL.

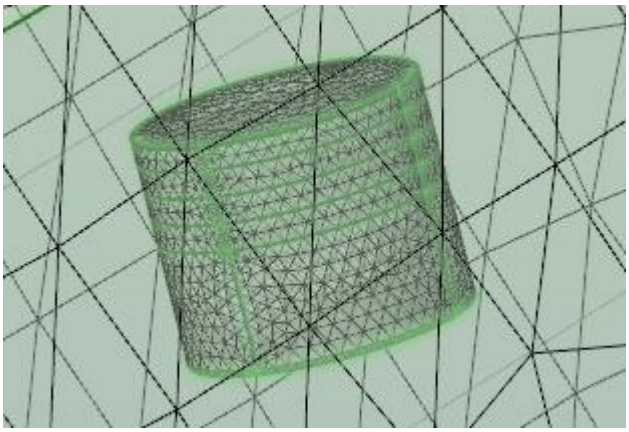

Figure 5.3. General view of solar pond in COMSOL.

Besides, the flow of water inside the pond and flow of air around the pond had to be specified inside the boundaries, which can be seen in Figure 5.4. For example, the wind speed was modeled in the program as air passing over the solar pond in a particular direction. Additionally, the convective heat transfer was established between the solar pond, and the water inside the pond, and the ambient air. To define these flows, heat transfer in fluids section was chosen on modeling for each defined fluid materials. This section was also used to specify the heat source within the domain.

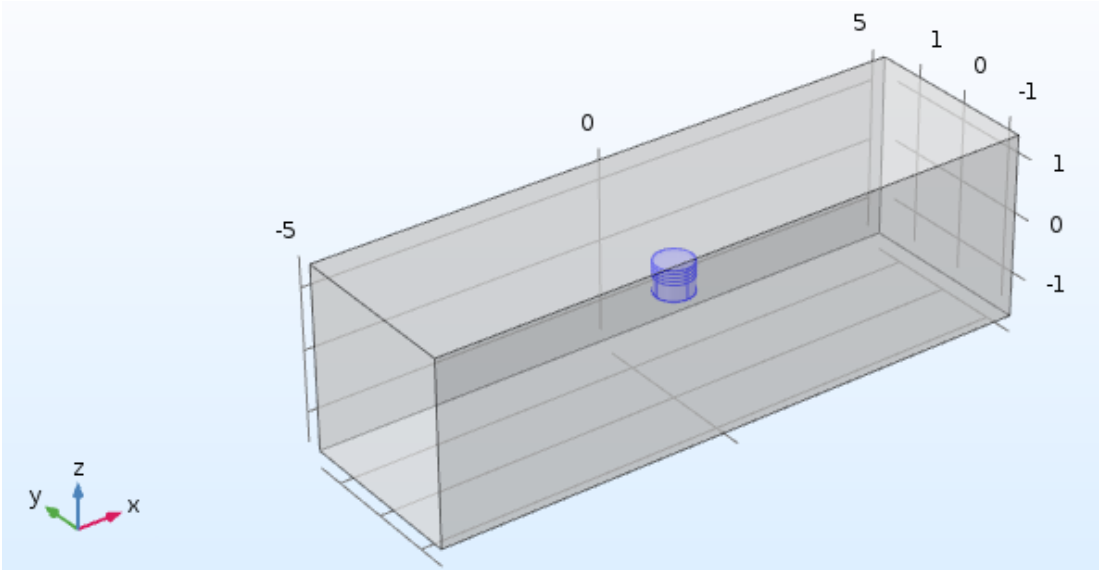

Figure 5.4. General view of boundaries to define the wind speed..

This model uses Equation (13) as the mathematical model for heat transfer in fluids.

$$\rho C_p \frac{\partial T}{\partial t} + \rho C_p u.\nabla T = \nabla.(k\nabla T) + Q \quad (13)$$

where ρ is the density, C_p denotes the fluid heat capacity at constant pressure, which defines the amount of heat energy needed to generate a unit temperature change in a unit mass, k represents the fluid thermal conductivity, u represents the fluid velocity, Q is the heat source as well as ∇T symbolizes the temperature gradient (Multiphysics, COMSOL., 2014).

Water and air were defined to the program as fluids 1 and 2, respectively. For both fluids, Equation (14) was used to obtain results:

$$\rho C_p \frac{\partial T}{\partial t} + \rho C_p u.\nabla T + \nabla q = Q + Q_p + Q_{vd} \quad (14)$$

$q = -k\nabla T$, where k denotes the thermal conductivity of the material.

In Equation (14), Q_p , Q_{vd} refer to the work because of pressure variance, and the viscous dissipation term, respectively.

Heat flux boundary condition was also specified for the insulation, which can be seen in Equation (15), where n denotes the normal vector of the boundary, q (in W/m^2) is the conductive heat flux vector, which is equal to $-k\nabla T$, and q_0 represents the inward heat flux that is generally the summation of heat transfer processes such as radiation, conduction or convection (Multiphysics, COMSOL., 2014).

$$-n.q = q_0 \quad (15)$$

However, if there is a thermal insulation, q_0 is equal to zero. In this thesis, insulation was used and defined on COMSOL, but there is convective heat transfer between the insulation and outside air; thus, heat flux could not be defined as zero.

Additionally, for the solid part, i.e., the pond and the insulation, energy equation can be demonstrated as below:

$$\rho C_p \frac{\partial T}{\partial t} + \rho C_p u.\nabla T + \nabla q = Q + Q_{ted} \quad (16)$$

where Q is the heat source and Q_{ted} is the thermoelastic damping.

Moreover, solar insolation reaching the pond surface was defined as a boundary heat source, and the energy equation can be shown in Equation (17).

$$-n.q = Q_b \tag{17}$$

$$Q_b = \frac{P_b}{A} \tag{18}$$

In Equation (18), P_b is the power, and A is the top surface area of the pond. Q_b was considered as global horizontal insolation, which is measured by a pyranometer in this study.

The main aim of using modeling is to estimate volume average temperature distributions of each layer for different conditions.

5.1 Volume Average Temperature

Volume average temperature can be calculated as:

$$T_{vol,avg} = \frac{T_1+T_2+\cdots+T_n}{n} \tag{19}$$

For each layer, representative thermocouple values are used to calculate volume average temperatures, which can be seen in Figure 3.2. Therefore, in Equation (19), "n" represents the number of thermocouples that are used. Calculated volume average temperatures obtained from the experimentation were used as inputs to the modeling.

5.2 Thermal Radiation Absorption

Absorption can be defined as a phenomenon which the thermal energy reduces while passing through the medium and because of that; this medium is usually called the absorbing medium. Additionally, the medium includes a lot of molecules which can absorb and emit thermal radiation rays (Siegel, 2001).

According to Siegel (2001), as monochromatic radiation, having wavelength (λ), transfers vertically via the medium with layer thickness of ds, the intensity of radiation, which is the amount of emitted energy per unit time from the surface area perpendicular to the direction of radiation is proportional to the intensity and it is shown in Equation (20).

$$\frac{dI_{\lambda,s}}{ds} = -K_{\lambda}\, I_{\lambda,s} \tag{20}$$

In Equation (20), proportionality constant is represented by K_{λ}, which is also known as "monochromatic extinction coefficient". However, in this thesis grey body assumption is used, where absorptivity and emissivity are independent of wavelength.

Equation (20) shows the radiation intensity attenuation per unit distance which is affected by both pressure and temperature. Furthermore, it involves not only absorption but also scattering impacts (Siegel, 2001).

If Equation (20) is integrated and radiation intensity is set to I_0 when the s is equal to zero; then Equation (21) is obtained.

$$I_s = I_0 \exp(-\int_0^s K\, ds) \tag{21}$$

In Equation (21), K is assumed to be constant and optical thickness is defined as δ_s is equal to the Ks, then monochrome transmissivity (τ_s) and absorptivity (α_s) are calculated by using Equation (22) and Equation (23).

$$\tau_s = \frac{I_s}{I_0} = \exp(-K\, s) = e^{-\delta_s} \tag{22}$$

$$\alpha_s = 1 - e^{-\delta_s} = 1 - \tau_s \tag{23}$$

The above equations shown in this section are useful to explain the effects of layer thicknesses on pond temperatures.

5.3 Heat Losses

Surface convection, radiative heat transfer, heat loss through the pond walls as well as heat transfer through the NCZ should be considered for the UCZ. It is known that NCZ is non-convective zone, and for this region heat loss through the walls as well as heat transfer through both UCZ and LCZ should be taken into account. Finally, both heat loss to the walls and ground, as well as heat transfer through NCZ should be considered for LCZ.

CHAPTER 6
RESULTS AND DISCUSSION OF NUMERICAL PART

This chapter includes 3 major parts. The first part contains the comparison of the estimated pond temperature using the simulation program with the experimental data. The second part examines the effects of weather condition on the temperature profile and the final part investigates the effects of pond geometry on the pond temperature.

6.1 Comparison between Experimental and Modeling Pond Temperature Profiles

Ambient temperature, relative humidity, wind speed, layer temperature, and insolation from five arbitrarily days, collected from experimental data, were used as inputs to the program as indicated in Table 6.1. Additionally, initial volume average temperatures of each layer for each specified day from experimental data was entered into the program. Then, simulation was performed for 10 minutes and 2 hours interval.

Table 6.1. Input values for the simulation part.

Day	Time	T_{amb} (ºC)	U_w (m/s)	GHI ($W \cdot h/m^2$)	RH (%)
18.04.2017	10:40	21.1	1.9	811.8	0.8
19.04.2017	13:30	20.5	5.5	977.1	0.4
24.04.2017	17:00	17.2	6.1	482.0	0.5
29.05.2017	09:00	23.5	2.0	622.4	0.7
17.06.2017	03:00	20.0	1.8	0.00	0.9

Based on these inputs (Table 6.1), program was run, and volume average temperatures were obtained for UCZ, LCZ and NCZ by using Equation (19).

Experimental data and the corresponding simulation results are shown in Table 6.2. Additionally, layer temperature differences between the experiment and modeling of the pond can be seen in Table 6.3. For the 10 minutes interval results, generally up to

±3ºC temperature difference in the temperature of UCZ, NCZ and LCZ between the simulation and the experiment were observed, which was in the calculated uncertainty range (about 3ºC), explained in Section 3.3.

According to the 10 minutes results, UCZ temperature values estimated by COMSOL were usually higher than the experimental data; however, they were close to the experimental data results.

Table 6.2. Experimental data and simulation results.

Day & Time			Experimental Data			COMSOL Results		
Day	Start time	End time	T_{LCZ}(ºC)	T_{NCZ}(ºC)	T_{UCZ}(ºC)	T_{LCZ}(ºC)	T_{NCZ}(ºC)	T_{UCZ}(ºC)
18.04.2017	10:40	10:50	26.2	21.4	18.3	26.2	22.3	21.0
18.04.2017	10:40	12:40	23.1	18.4	15.0	25.0	22.5	22.6
19.04.2017	13:30	13:40	27.6	22.0	16.9	26.1	21.7	19.7
19.04.2017	13:30	15:30	28.6	22.3	16.5	24.7	21.8	21.0
24.04.2017	17:00	17:10	32.6	23.6	17.7	30.2	23.1	18.3
24.04.2017	17:00	19:00	37.1	26.6	19.5	27.0	22.4	18.4
29.05.2017	09:00	09:10	26.0	16.0	13.5	25.7	17.2	18.6
29.05.2017	09:00	11:00	26.7	17.5	15.6	24.9	19.0	22.0
17.06.2017	03:00	03:10	41.5	36.2	27.5	38.4	34.6	25.6
17.06.2017	03:00	05:00	41.6	36.3	27.4	34.2	32.2	23.7

Table 6.3. Temperature differences between experimental data and simulation results.

Day & Time		Temperature differences between the model and experiment		
Day	Time	ΔT_{LCZ} (ºC)	ΔT_{NCZ} (ºC)	ΔT_{UCZ} (ºC)
18.04.2017	10:50	0	0.9	2.7
18.04.2017	12:40	1.9	4.1	7.6
19.04.2017	13:40	1.5	0.3	2.8
19.04.2017	15:30	3.9	0.5	4.5
24.04.2017	17:10	2.4	0.5	0.6
24.04.2017	19:00	10.1	4.2	1.1
29.05.2017	09:10	0.3	1.2	5.1
29.05.2017	11:00	1.8	1.5	6.4
17.06.2017	03:10	3.1	1.6	1.9
17.06.2017	05:00	7.4	4.1	3.7

Parameters were investigated individually to gain insights of these results. For instance, high GHI resulted in increasing the UCZ temperature differences between simulation results and experimental data, which was about 3ºC. On the 18th and 19th April, daily total GHI was higher than the other selected days, which was recorded as about 812 and 977 Wh/m^2, respectively, and on these days, ambient temperatures were also found as about 21ºC and 20.5ºC, respectively (Table 6.1). It was observed that UCZ temperatures that were taken from experimental data were about 3ºC lower than

the ambient temperature. It is understood that most of the solar insolation initially absorbed in the UCZ, and some part of the absorbed heat by UCZ is lost due mainly to the convection heat transfer to the surrounding air. In other words, lower UCZ temperatures on the experimental results might be explained by heat loss through the outside of the solar pond. On the other hand, according to the simulation results, UCZ temperatures were close to the ambient air temperatures that were found as approximately 21ºC and 20ºC, since model assumes that no evaporation and no salt diffusion occur during the process.

Additionally, although the wind speed on 19th April was three times higher than the 18th of April, recorded as almost 6 m/s, the UCZ temperature difference between simulation results and experimental data remained almost the same, which was about 3ºC. This was because of the high GHI on these days. Similarly, there was also 6 m/s wind speed on 24th April, which was nearly the same as that of 19th April. However, lower UCZ temperature difference, 0.6 ºC, which was insignificant, was obtained on 24th April, which might be because of the lower solar insolation, 482 Wh/m^2 that reached to the upper layer of the SGSP. As a result, if the solar insolation increases, temperature difference between the simulation program and experimental data also increases on UCZ and vice versa.

Furthermore, although there was no solar insolation on 17th June at 3:10 am, UCZ temperature was found to be higher than the ambient temperature (20ºC) those experimentally (27.5ºC) and using simulation (25.6ºC). Furthermore, high LCZ temperatures were obtained in both experimental data and COMSOL; almost 42ºC and 35ºC, respectively. Thus, heat transfer that might have occurred through the upper layer, may have resulted in obtaining higher UCZ temperatures than expected. Besides, it can be observed that NCZ temperatures in both experimental and modeling results were close to each other on 17th June at 3 am. As a result, even if there was no solar radiation, solar pond continued to operate properly.

As mentioned before, the simulation was run based on the initial values of some variables, and the program assumed that these variables do not change with the time. This is the main reason for obtaining lower temperature differences between the layers for 10 minutes results (Table 6.3) since there was no profound change in the layer temperatures during this short interval. However, high temperature differences were

observed during the 2-hour intervals. For example, one of the highest UCZ temperature differences between the simulation result and experimental data, was found to be 8ºC, obtained on 18th April.

Figure 6.1 shows the temporal changes of the solar insolation, wind speed and ambient temperature between 10:40 am and 12:40 pm. According to Figure 6.1, it has been observed that ambient temperature did not change significantly. For instance, when the wind speed increased from 2.4 m/s to 4.7 m/s from 11:00 am to 11:30 am, ambient temperature decreased from 22ºC to 20ºC. However, it was observed that GHI did not remain constant during this period. At the beginning 800 W/m^2 of GHI was recorded, and then it had started to increase until at almost 12 pm when the highest amount of solar radiation (977 W/m^2) reached to the surface of the pond. However, a sharp decline on GHI was observed from 11:50 am to 12:10 pm which decreased to almost 470 W/m^2. The decrease in the amount of solar radiation reaching to the pond surface directly resulted from obtaining lower UCZ temperatures.

Additionally, wind speed started to increase from 3.5 m/s to almost 7.5 m/s after at solar noon which might have also reduced the UCZ temperature. These observations might explain for obtaining lower UCZ temperature (about 15ºC) for the experimental analysis on 18th April, while UCZ temperature was found to be about 23ºC on COMSOL which was close to the ambient temperature. As a result, the temperature gradient between the UCZ and LCZ in experimental results, which was calculated as 8ºC, was higher than the results of COMSOL that was measured as 2.4ºC. The main reason for this difference was that the program assumes no variances on the inputs during this period (2 hours); however, in reality, there were some significant variations that affect the layer temperatures as shown in Figure 6.1.

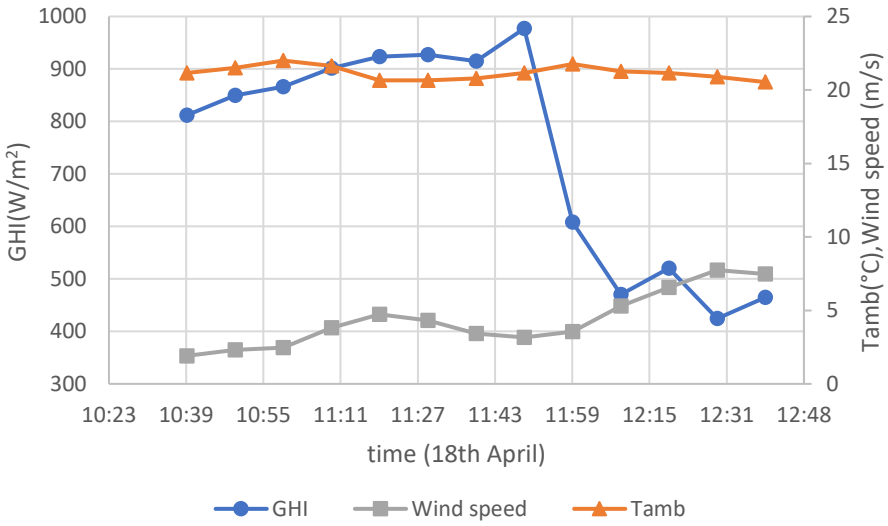

Figure 6.1. Variances between GHI, wind speed and ambient temperature on 18th April.

Furthermore, one of the smallest LCZ and NCZ temperature difference between the experimental result and the simulation result was obtained on 29th May, which might be because of the high heat capacity of these layers. As before, inputs were investigated for 2-hour intervals, as shown in Figure 6.2. COMSOL assumed that GHI was constant during this interval which was 600 W/m^2. However, it reached its highest value which was almost 1000 W/m^2 at 10:50 am, then it followed a decreasing pattern and finally, GHI reached at 717 W/m^2 at 11:00 am during the experiment.

According to Figure 6.2, the wind speed was measured at almost 2 m/s at 9:00 am and increased to about 6 m/s until 9:50 am. Then, its speed was almost constant during the whole period. However, it was observed that increasing wind speed did not have much effect on both LCZ and NCZ temperatures. However, it caused to decrease the UCZ temperature since there was a high heat loss from the surface of the pond through the outside due to the high wind speed. UCZ temperature was measured as about 16ºC at the end of 2 hours period; thus, the temperature gradient between UCZ and LCZ was higher (almost 11ºC) based on experimental data than the simulation result (about 3ºC).

Moreover, UCZ temperature in the simulation program (22ºC) was close to the ambient temperature (23.5ºC), which might be because of the model assumption including no evaporation, explaining the lower temperature gradient between the bottom and top layer.

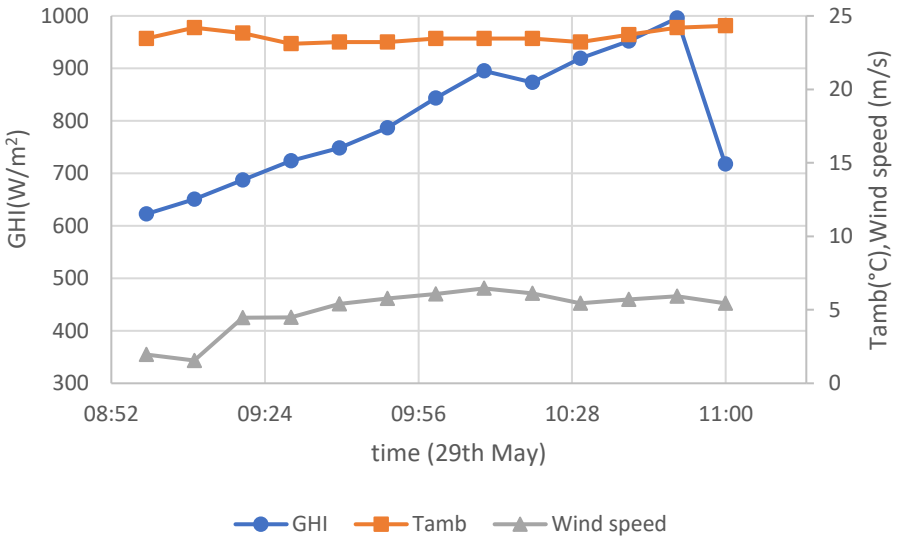

Figure 6.2. Variances between GHI, wind speed and ambient temperature on 29th May.

Another interesting result was seen on 24th April, when the smallest UCZ temperature difference (1.1ºC) between COMSOL and experimental results was obtained. Based on Figure 6.3, GHI followed a decreasing pattern and wind speed was usually measured as considerably high as about 6-7 m/s, which might have decreased UCZ temperature. Furthermore, the unchanged ambient temperature during these two hour periods might be one of the reasons for having small temperature differences between experimental and simulated results.

It is known that when the wind speed increases, water mass transfer coefficient on the pond surface also increases which is resulted in increasing the evaporation rate. If the evaporation rate on the surface increases, temperature will start to decrease in each zone. Thus, it should have been expected to obtain higher UCZ temperature gradient between experimental data and the simulation results. However, UCZ temperature was found nearly as 19.5ºC, which was slightly higher than the ambient temperature that was recorded as 17.2ºC. Salt diffusion through the upper layer might be the reason for this increase. Similarly, required surface washing was not done on this day which might have been another reason since it can help to keep the water level in the pond constant against the evaporation loss due to the high wind velocity.

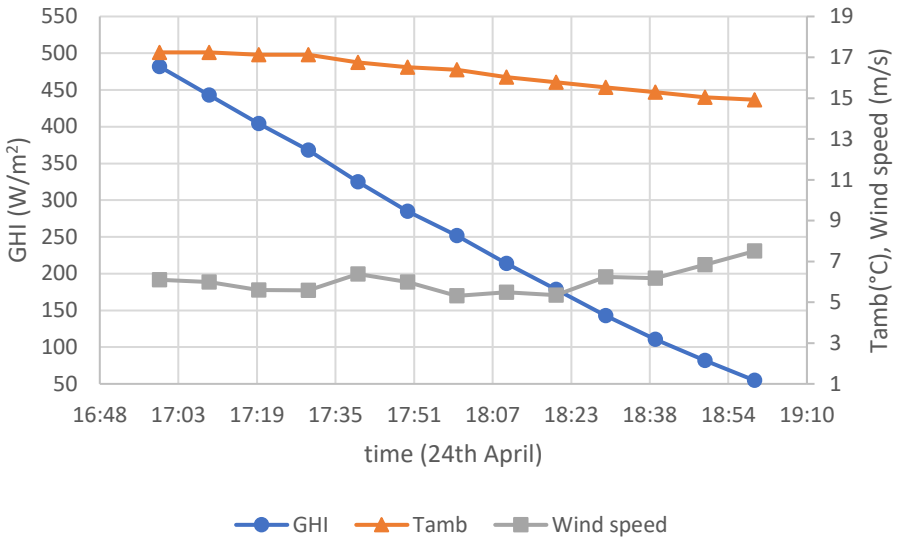

Figure 6.3.Variances in between GHI, wind speed and ambient temperature on 24th April.

6.2 Parametric Study 1: Effects of Climate Condition on Pond Temperatures

This parametric study investigated the effects of climate conditions including global horizontal insolation (GHI), wind speed and ambient temperature on the layer temperatures. Simulations were run using experimental data including ambient temperature, wind speed and initial temperature values of each layer at 10:40 am on 18th April, and the pond was simulated for 3 hours (10800 minutes) for each parameter.

6.2.1 Effects of Global Horizontal Insolation

First, the effect of GHI was investigated. Based on the obtained results, temperatures of UCZ, NCZ and LCZ were created, which are shown in Figure 6.4, Figure 6.5 and Figure 6.6, respectively.

Different energy flow paths including heat transfer such as conduction, convection or radiation directly affect the temperature profiles in a salt gradient solar pond, and one of the most important effects is the solar radiation. Thus, net solar energy absorbed by each layer specifies the thermal behavior of a SGSP (Enshayan, 1989).

It is known that incoming solar radiation initially absorbed in UCZ, and some part of it pass through NCZ providing to increase its temperature. According to simulation results, both UCZ and NCZ temperatures increase with increasing solar insolation. Figure 6.4 shows the variations of UCZ temperatures with time. Based on that, it can

be easily seen that the temperature of UCZ increases with time for each defined GHI. The main reason is that the volume of UCZ has the smallest amount, which is 15 liters and since GHI first contact with UCZ; its temperature rises both easily and quickly. Furthermore, it was observed that variations of surface layer temperature were higher than the other layers since the penetration of solar insolation occurs easily in this layer. After about 10 minutes run of simulation program, each UCZ temperatures were similar to ambient air temperature (21.1°C), which were 20.2°C, 20.7°C and 21.2°C with increasing GHI, of 100 W/m^2, 500 W/m^2, and 900 W/m^2, respectively. However, at the end of 3 hours, the maximum UCZ temperature reached about 23°C when GHI was defined as 900 W/m^2, which was the highest amount, whereas the minimum temperature of about 21.2°C was obtained at the lowest amount of GHI, 100 W/m^2. Hence, the highest UCZ temperature gradient, nearly 2.4°C, occurred at 900 W/m^2 of solar insolation while the smallest UCZ temperature difference, 0.99°C was seen at 100 W/m^2. As a result, when the incoming solar radiation increased, temperature gradient of UCZ also increased as expected as shown in Figure 6.4.

Furthermore, according to the simulation results, when 900 W/m^2 of GHI was defined to the program; the surface layer temperature passed NCZ temperature after 4800 seconds. It is known that meteorological conditions can easily affect the surface layer temperature, and as a result, at the end of 3 hours, UCZ temperature (23.1°C) was found to be higher than NCZ temperature (22.6°C).

On the other hand, the temperature of LCZ followed a decreasing pattern with all given GHI, which can be seen in Figure 6.6. This result showed that enough incoming solar radiation cannot reach the lower convective zone, which can be explained by the attenuation of downward irradiance with increasing penetration depth. It was observed that temperature gradient of LCZ between 10 minutes and 3-hour intervals were calculated as about 1.5°C for each given GHI, which might be clarified by both heat loss from the pond wall and ground. However, it was observed that although GHI cannot reach the lower layer radiatively, it mostly protected its temperature due to its high heat capacity.

As mentioned above, NCZ temperature increased with increasing solar insolation, as shown in Figure 6.5. However, these increases were very slight for 3 hours interval,

which changed from 0.03°C to 0.41°C. Again, it can be explained by the decreasing effect of GHI with increasing depth.

As known that in a salt gradient solar pond, NCZ contains salt gradient which prevents circulation inside the pond and behaves as insulation for the LCZ. If this gradient is properly achieved, convective motion is suppressed, and thermal energy can be absorbed in LCZ. Additionally, when the incoming solar radiation reaches the bottom layer of the pond, it heats the concentrated brine providing not to rise outside the LCZ, which can be explained by the greater effect of salinity on density than the impact of temperature. In general, it is expected to obtain higher LCZ temperature values with the increasing GHI or vice versa. However, based on simulation results, GHI cannot penetrate through both NCZ and LCZ to bring about an effective change on the bottom layer temperature. Therefore, based on COMSOL results, the overall efficiency of SGSP might be low because the temperature of LCZ does not change effectively.

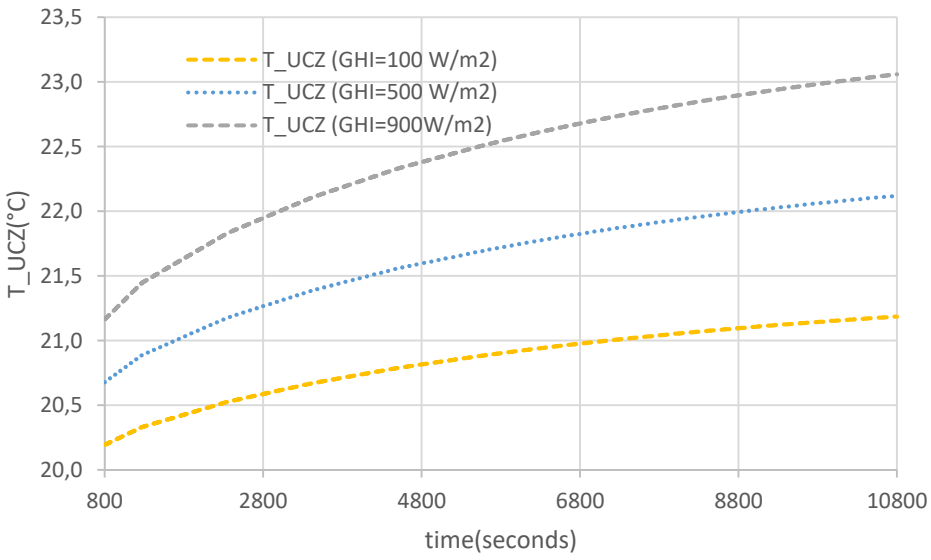

Figure 6.4. Effect of GHI on the temperature of the upper convective zone.

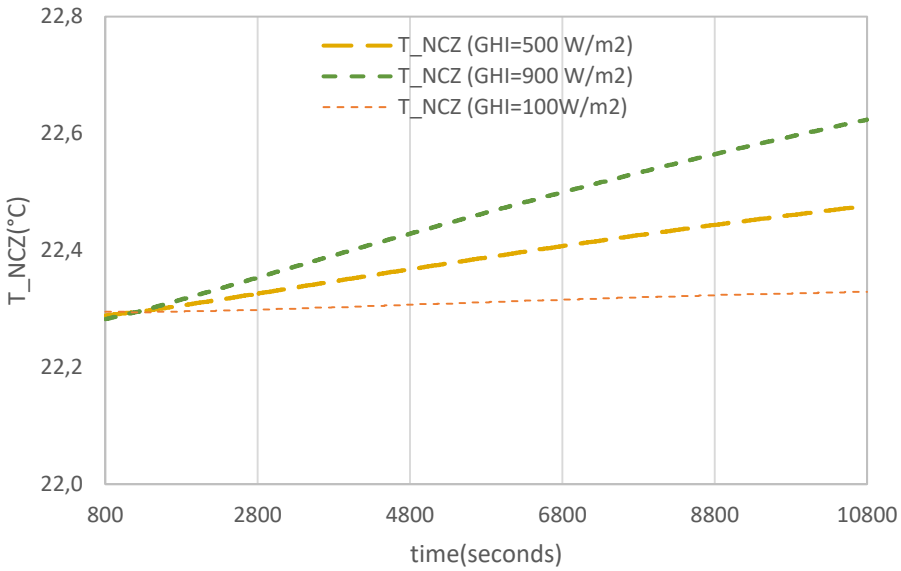

Figure 6.5. Effect of GHI on the temperature of the non-convective zone.

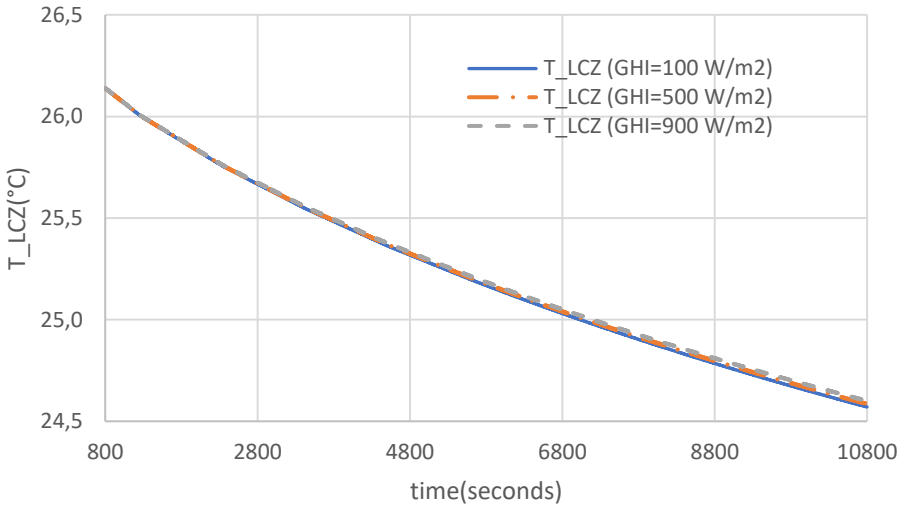

Figure 6.6. Effect of GHI on the temperature of the lower convective zone.

6.2.2 Effects of Wind Speed

Secondly, the effect of wind speed on layer temperatures was investigated. Depending on obtained results from the simulation program for both 800 seconds and 10800 seconds, shown in Table 6.4, plots of UCZ, NCZ and LCZ temperatures with various wind speeds are shown in Figure 6.7, Figure 6.8 and Figure 6.9, respectively.

Simulations were performed at constant GHI of 811.8 W/m^2 and air temperature of 21.1°C on 18th April, just wind velocity was changed as a parameter.

Differences between the top and bottom layer temperatures were calculated as 0.3°C, 2.4°C, 2.8°C, 3.0°C, 3.1°C and 3.2°C, respectively with increasing wind speeds as follows of 1 m/s, 3 m/s, 5 m/s, 7 m/s, 9 m/s and 11 m/s. It is expected to have higher temperature difference between LCZ and UCZ, when the velocity of wind speed increases since at higher wind speeds, UCZ temperature starts to decrease due to higher convective heat losses to the ambient air. As a result, the maximum temperature difference (3.2°C) was maintained at the highest wind speed of 11 m/s, whereas the minimum temperature gradient (0.3°C) was obtained at the lowest wind speed which was 1 m/s. On the other hand, these ΔT differences between LCZ and UCZ were mostly close to each other that can be explained by decreasing solar insolation which is able to reach the bottom layer. In other words, decreasing effect of downward irradiance with the increasing penetration depth might prevent increasing temperature level in the bottom layer. Moreover, there was also heat loss from side walls, ground as well as through the outside which had to be considered. If wind speed increased, UCZ temperature started to decrease due to the both high heat and evaporation losses. However, the model assumed that there was no evaporation; thus, when the wind speed increased, heat loss through the atmosphere increased which has resulted in obtaining lower UCZ temperature as shown in Figure 6.7.

Additionally, temperature variations within NCZ layer after 13 minutes and 3 hours were mostly found as similar values, which changed from 0.58°C to 0.02°C (change was insignificant) when the wind speed increased from 1 m/s to 11 m/s. For example, the minimum temperature difference within NCZ was maintained when the wind velocity was equal to 1 m/s, whereas the maximum temperature gradient was observed when the wind velocity was equal to 11 m/s. Therefore, increase in the temperature gradient was observed with increasing wind speed, in other words, NCZ temperatures increased at lower wind speeds, which can be seen in Figure 6.8. However, it mostly protected its temperature for all conditions since temperature gradients were very small.

Furthermore, LCZ temperatures decreased with each defined wind speeds for the duration of 3 hours. Attenuation on the solar irradiance reached through LCZ might be

the main reason for this, because it lost its effect with increasing depth. Another reason might be because of heat loss from ground and side walls. Based on Figure 6.9, the highest LCZ temperature was obtained at the lowest wind speed whereas the lowest LCZ temperature was maintained at the highest wind speed. On the other hand, LCZ mostly kept its temperatures the same for all conditions, which might be explained by the high heat capacity of this layer. Although variations of LCZ temperatures were very close to each other at all wind speeds, LCZ temperatures decreased by 1.4°C, 1.56°C, 1.56°C, 1.57°C, 1.57°C and 1.57°C, respectively, when the wind speed was 1, 3, 5, 7, 9 and 11 m/s.

As a result, wind speed mostly affects UCZ temperature, whereas it does not have a profound effect on both NCZ and LCZ temperature profiles.

Table 6.4. Variations of layer temperatures with wind speed.

	800 seconds			10800 seconds		
Uw (m/s)	T_LCZ(°C)	T_NCZ(°C)	T_UCZ(°C)	T_LCZ(°C)	T_NCZ(°C)	T_UCZ(°C)
1	26.2	22.3	21.6	24.7	22.9	24.4
3	26.1	22.3	20.8	24.5	22.5	22.2
5	26.1	22.3	20.6	24.5	22.4	21.7
7	26.1	22.3	20.5	24.5	22.3	21.5
9	26.1	22.3	20.4	24.5	22.3	21.4
11	26.0	22.3	20.4	24.5	22.3	21.3

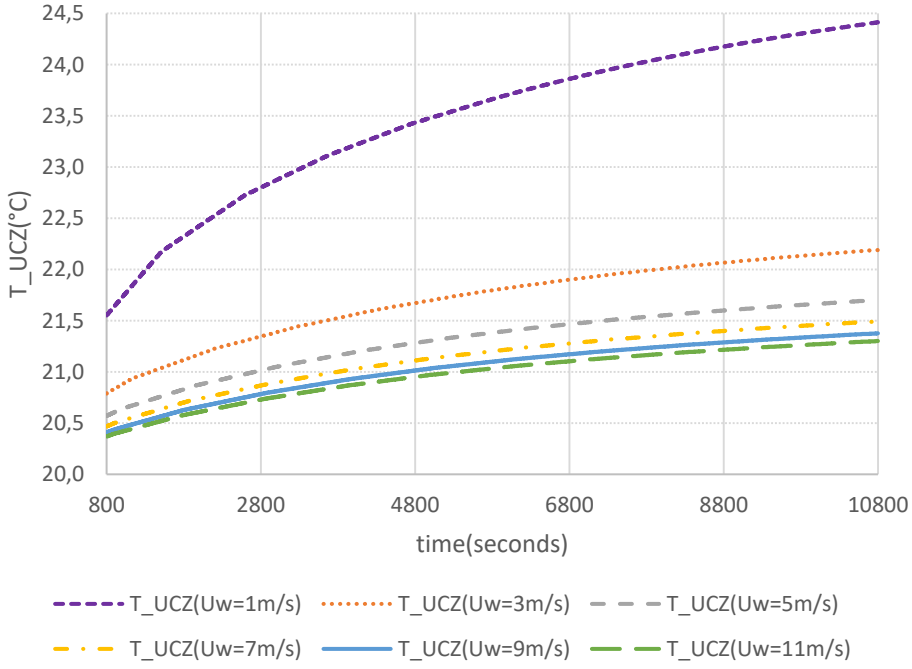

Figure 6.7. Effect of wind speed on the temperature of the upper convective zone.

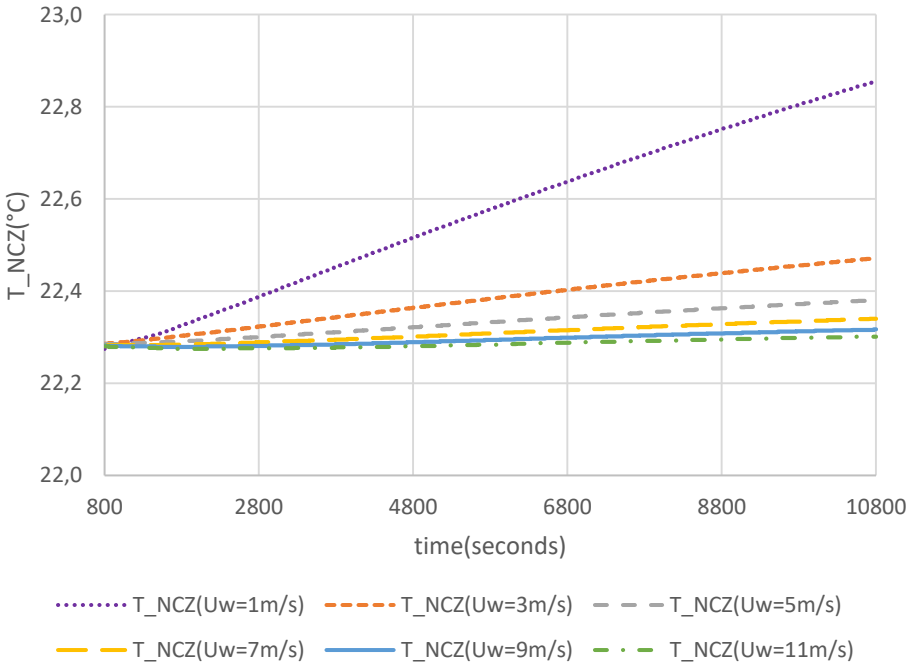

Figure 6.8. Effect of wind speed on the temperature of the non-convective zone.

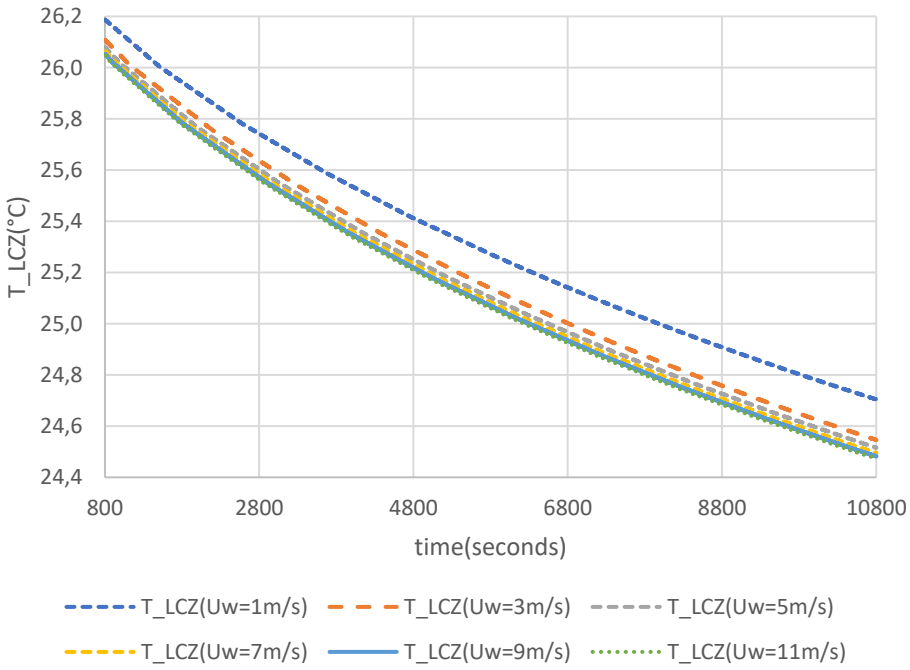

Figure 6.9. Effect of wind speed on the temperature of the lower convective zone.

6.2.3 Effects of Ambient Temperature

Finally, the effect of ambient air temperature on the layer temperatures was examined. Table 6.5 shows the obtained results from the simulation program for both 800 seconds and 10800 seconds. After that, plots of UCZ, NCZ and LCZ temperature with ambient temperature were plotted in Figure 6.10, Figure 6.11 and Figure 6.12, respectively

When the ambient temperature was at its lowest value (10°C) UCZ temperature started to reduce because UCZ temperature was affected easily by the meteorological conditions; thus, it lost its heat to outside convectively. About 1.7°C of the reduction in the temperature of UCZ was seen when the ambient temperature was equal to 10°C according to the simulation results. After 10°C, increase in ambient temperatures were resulted in rising UCZ temperature, as shown in Figure 6.10. These increases were calculated as 1.4°C, 4.3°C and 7.6°C with rising ambient temperatures of 20°C, 30°C and 40°C, respectively. The maximum increase in UCZ temperature which was recorded as about 8°C, was observed at the highest ambient temperature. Hence, when ambient temperatures started to increase, UCZ temperatures also increased.

Furthermore, except for ambient temperature of 10°C, NCZ temperatures increased with increasing ambient temperature. These variations were found as 0.01°C, 2.31°C and 4.61°C with respect to ambient temperatures of 20°C, 30°C and 40°C, respectively. As for the case of UCZ, the maximum increase in NCZ was measured at ambient temperature of 40°C. Similarly, by looking at the variations on LCZ temperatures, temperature increases were seen after 30°C, as shown in Figure 6.12. Furthermore, the bottom layer temperature increased from 0.6°C to 3.0°C, as the ambient temperature increased from 30°C to 40°C. However, for the ambient temperatures lower than 20°C, the LCZ temperatures decreased. For example, LCZ temperature decreased from 25.9°C to 24.1°C, at ambient temperature of 20°C after 10800 seconds. Similarly, nearly 4°C reduction in LCZ temperature was obtained, when the ambient temperature was the lowest value, which was equal to 10°C.

As a result, ambient temperature had the highest effect on the layer temperatures, since the highest temperature variations were observed with changing ambient temperatures.

Table 6.5. Variations of layer temperatures with ambient temperature.

	800 seconds			10800 seconds		
Tamb(°C)	T_LCZ(°C)	T_NCZ(°C)	T_UCZ(°C)	T_LCZ(°C)	T_NCZ(°C)	T_UCZ(°C)
10	24.5	21.3	16.0	20.3	19.1	14.3
20	26.0	22.2	20.5	24.1	22.2	21.9
30	27.4	23.0	25.0	28.0	25.3	29.2
40	28.9	23.9	29.5	31.9	28.5	37.1

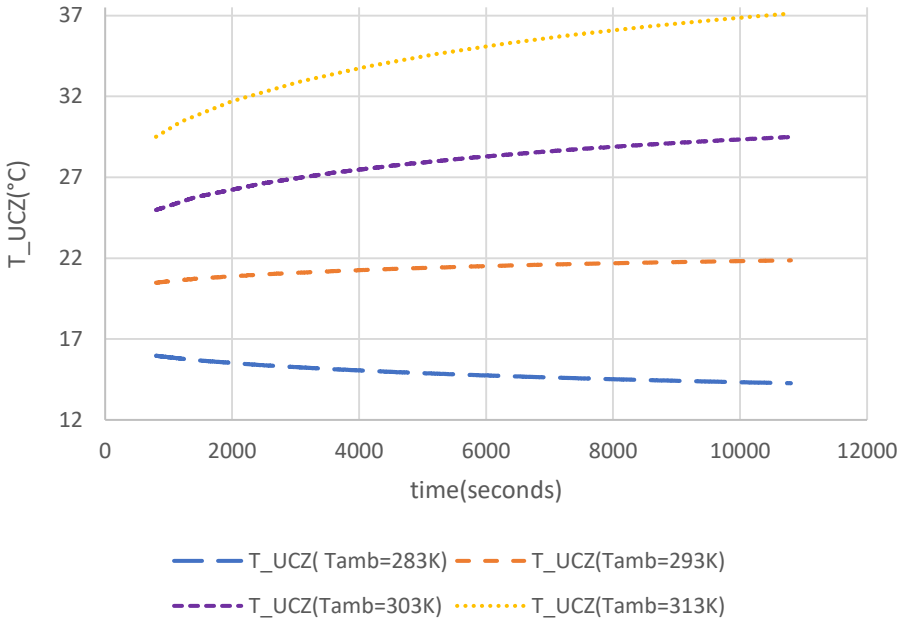

Figure 6.10. Effect of ambient temperature on UCZ temperature.

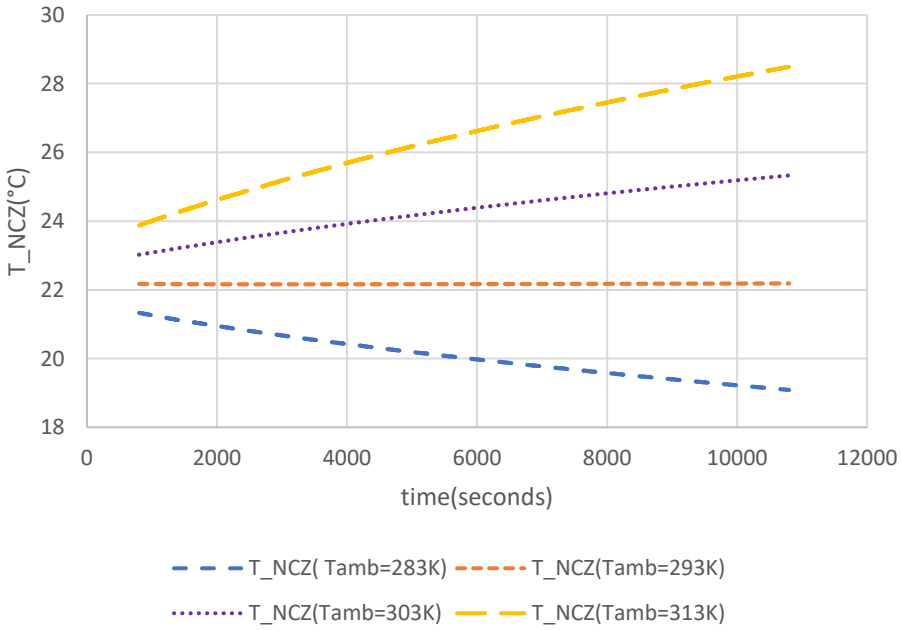

Figure 6.11. Effect of ambient temperature on NCZ temperature.

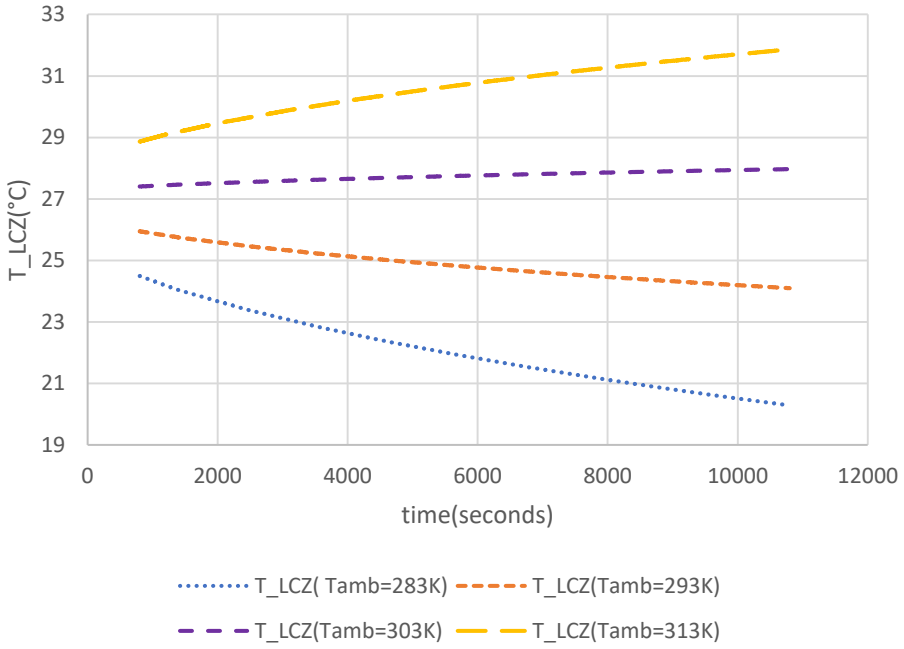

Figure 6.12. Effect of ambient temperature on LCZ temperature.

6.3 Parametric Study 2: Effects of Pond Geometry on Layer Temperatures

This section examined the effects of pond geometry including diameter and thicknesses on the layer temperatures. Simulations were run by using experimental data including incoming solar radiation, ambient temperature, wind speed and initial temperature values of each layer at 10:40 am on 18th April and it was operated at uniform intervals for 2 hours (7200 minutes) for each parameter.

6.3.1 Effects of Diameter

Firstly, the effect of diameter (from 35 cm to 80 cm) at uniform intervals of 15 cm, was investigated. Table 6.6 shows the results of temperatures obtained by COMSOL. Similarly, Figure 6.13, Figure 6.14 and Figure 6.15 show the effect of diameter on temperatures of LCZ, NCZ and UCZ, respectively, during 2 hours. Temperature gradients of each layer were found to be nearly the same which can be explained by the heat equation (Equation (24)), where heat loss is assumed to be negligible.

$$Q\ (J) = I(\frac{W}{m^2})\ A(m^2)\ t(s) = m(g)\ c_p(\frac{J}{g.°C})\ \Delta T(°C) \quad (24)$$

where area (A) and mass (m) that were required for Equation (24) were calculated, respectively, as,

$$A = \pi r^2 \quad (25)$$

$$m = \rho A h \quad (26)$$

where ρ is the density of water, A is the surface area of the pond and h is the overall height of the solar pond.

Thus, the amount of thermal energy can be calculated by using Equation (27), and it depends on mass (g), change in temperature (°C), and specific heat (J/g·°C). Additionally, incoming solar radiation that incident on a surface area at a specific time gives the thermal energy.

$$I (\pi r^2) t = m c_p \Delta T \quad (27)$$

Incoming solar radiation and specific heat were constant for 2 hours. Similarly, the height of each layer was not changed, and the density was constant; thus, mass changed only with the area. It is known that area increases with increasing diameter, and it resulted in increasing mass. Therefore, it was expected to obtain almost unchanged temperature gradient during this interval.

Table 6.6. Effect of diameter on layer temperatures.

	At the beginning			After 7200 seconds		
Dia (cm)	T_LCZ(°C)	T_NCZ(°C)	T_UCZ(°C)	T_LCZ(°C)	T_NCZ(°C)	T_UCZ(°C)
35	26.8	22.5	19.7	25.4	22.7	23.0
50	26.7	22.5	19.7	24.9	22.6	23.0
65	26.7	22.5	19.7	25.2	22.6	23.8
80	26.8	22.5	19.7	25.4	22.6	23.0

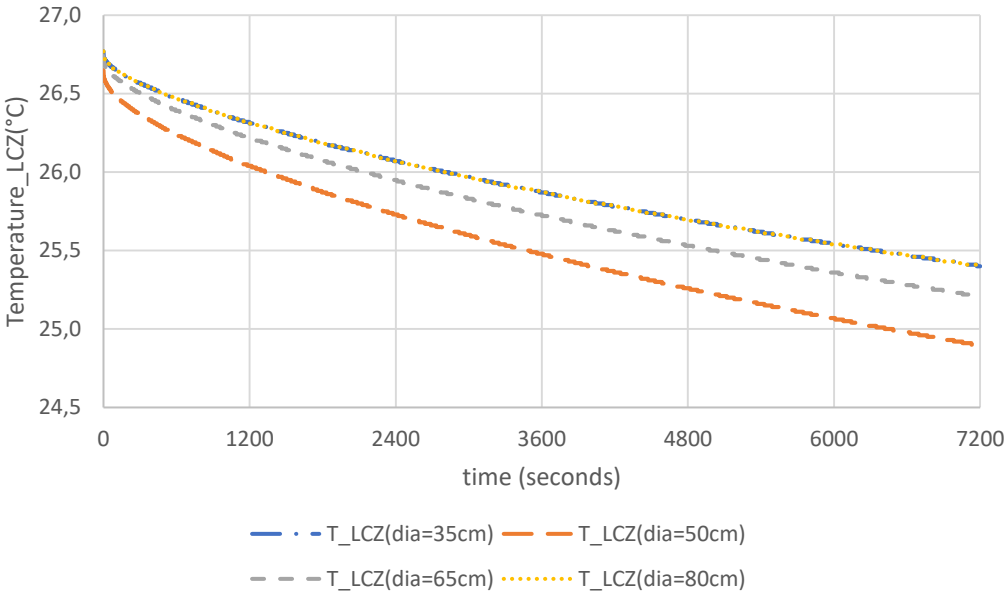

Figure 6.13. Temperature of LCZ with various diameters.

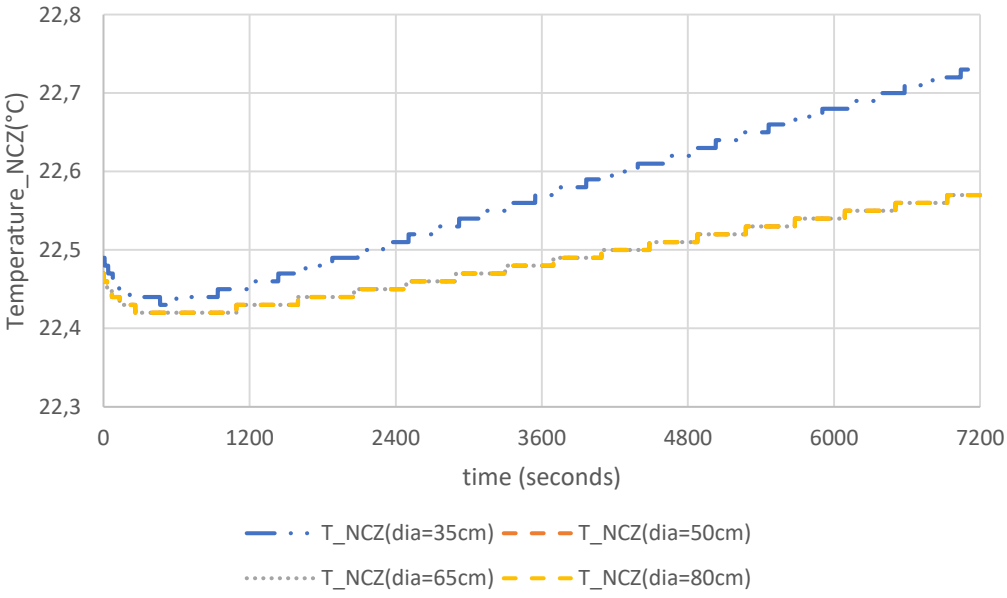

Figure 6.14. Temperature of NCZ with different diameters.

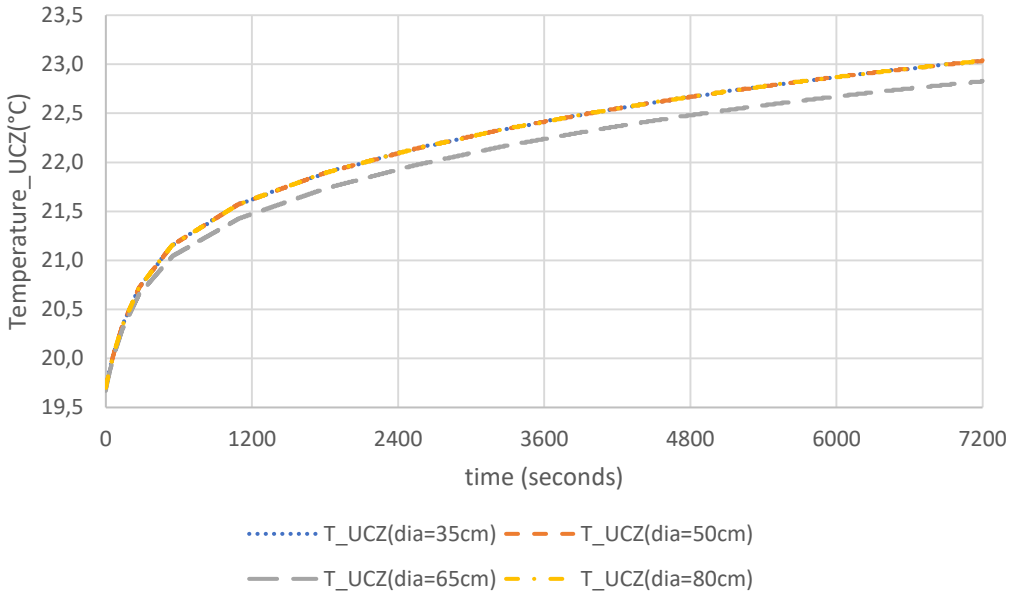

Figure 6.15. Temperature of UCZ with different diameters.

6.3.2 Effects of Layer Thicknesses

Secondly, the effects of layer thicknesses on layer temperatures were investigated by COMSOL. Total height was not changed, which was 55 cm. Layer thicknesses were arranged from ¼ to ¾ of the total height, which can be seen in Table 6.7. After that, the program was run and temperature versus time graphs for each layer was obtained, which are shown in Figure 6.16, Figure 6.17 and Figure 6.18, respectively.

According to obtained results, both NCZ and UCZ volume average temperatures varied exactly the same when the thicknesses were changed. The model was operated at a constant ambient temperature (21°C), wind speed (1.9 m/s) and global horizontal insolation (812 W/m^2). The maximum temperature increase was obtained in UCZ temperatures, which varied from about 20°C to 25°C, since no evaporation was assumed by the model; it was expected to obtain the highest temperature variations in the surface layer. As mentioned in Chapter 2, determination of layer thicknesses was very crucial for the solar pond mechanism. Briefly, when UCZ thickness increases, the amount of solar radiation that reaches the lower zones decreases. Hence, it was expected to obtain higher UCZ temperature in Case 1 than Case 2. On the other hand, in both cases, the temperature gradient in UCZ was similar, which can be seen in Figure 6.18. Although the difference between the two cases was about 5 cm, the UCZ height did not change much in both cases in general. For example, the temperature

changes at the top and the bottom points of UCZ decreased from 25.1°C to 24.2°C in the first case, whereas in the second case it dropped from 24°C to 20.2°C. Thus, an increase in the height resulted in decreasing effect of solar radiation, which is explained in Section 5.2. On the other hand, similar volume average temperature values in the UCZ were found by the model. Since GHI can easily reach through UCZ layer, the fastest and highest temperature variations were obtained in the surface layer, which might be the main reason to obtain unchanged volume average temperature variations in UCZ with time.

Additionally, thickness of NCZ is also important because it can directly affect the solar insolation reaching through LCZ. Thus, increase in thickness of NCZ is resulted in increasing insulation quality of this layer, but solar radiation reaching through LCZ reduces. Therefore, it was expected to get lower NCZ temperatures in Case 2 than the temperatures of Case 1, since its total height was higher when it was compared to the other case. However, again similar temperature gradients found as 1.5°C, were maintained in both cases, which are shown in Figure 6.17. Thus, it can be understood these adjusted thicknesses illustrated in Table 6.7 did not have a huge impact on the obtained NCZ temperatures.

Moreover, if the thickness of LCZ increases, thermal efficiency of the pond might reduce because the amount of heat losses through the side walls, ground as well as above layers of the pond might increase. Hence, adjustment of the thickness of LCZ was also crucial. It can be observed that LCZ temperature remained constant at about 26.8°C in Case 1, whereas temperature of LCZ decreased from 26.8°C to 25.5°C in Case 2, as shown in Figure 6.16. Normally, it was expected to reduce LCZ temperature in Case 1, since it has a more peripheral surface area that can contact and lose its heat. However, the layer temperature remained constant, which might be explained by the high heat capacity. Furthermore, lower LCZ temperature in Case 2 might be due to the heat loss and downward irradiance with increasing penetration depth. As a result, each layer thickness plays an important role on solar pond working mechanism; thus, determination of these heights should be done properly.

Table 6.7. Adjusted layer thicknesses.

Case Number	Height of LCZ (cm)	Height of NCZ_3 (cm)	Height of NCZ_2 (cm)	Height of NCZ_1 (cm)	Height of UCZ (cm)
1	41.25	2.41	2.41	2.41	2.02
2	13.75	9.59	9.59	9.59	7.98

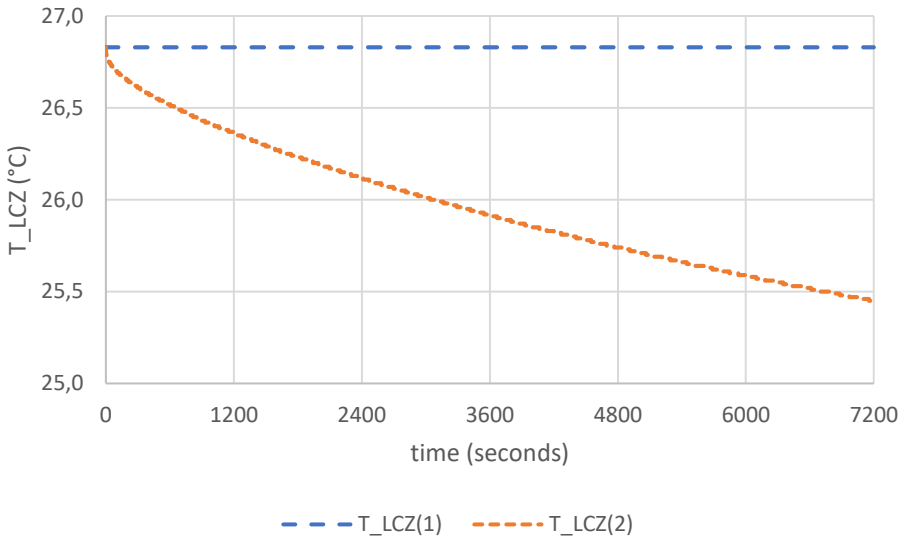

Figure 6.16. LCZ temperatures with different layer thicknesses.

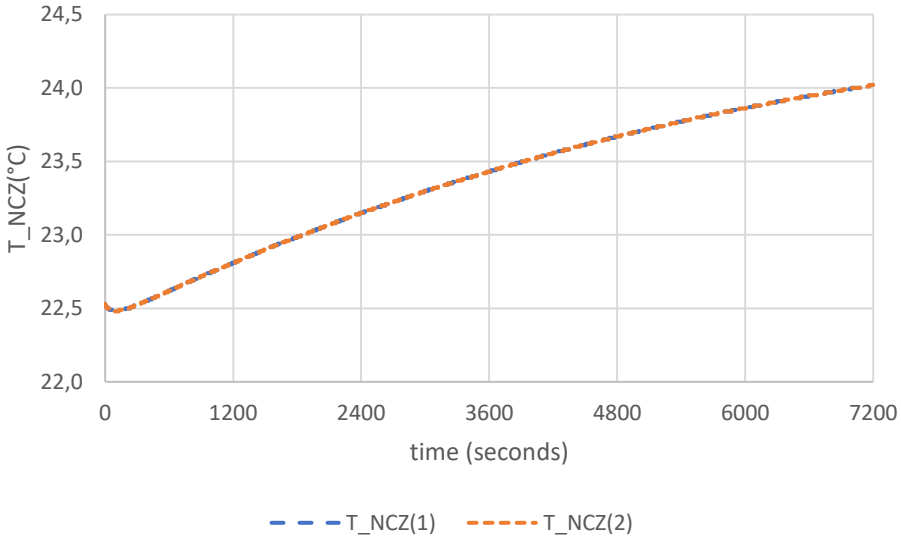

Figure 6.17. NCZ temperatures with different layer thicknesses.

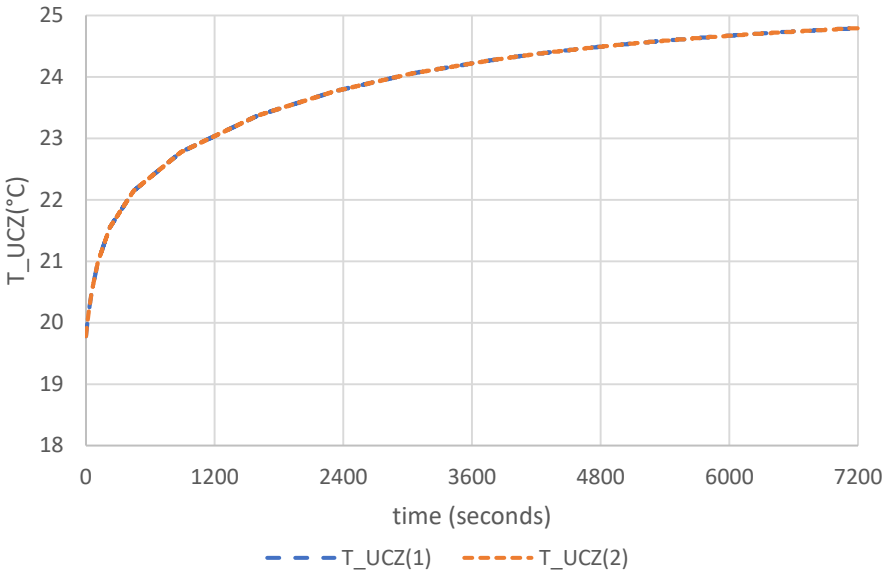

Figure 6.18. UCZ temperatures with different layer thicknesses.

CHAPTER 7
CONCLUSIONS AND RECOMMENDATIONS

SGSP has been thought as a low-cost solar energy system which collects solar radiation and stores it in the form of thermal energy. Additionally, it has been developed in years since it can be thought as a large-scale energy collector for a long-term use with no or little maintenance and no environmental hazard. Moreover, since its mechanism depends on clean and renewable energy, SGSP can be thought as a sustainable alternative for conventional energy sources. Although climatological conditions either variations in incoming solar radiation or wind speed can directly affect the thermal performance of the pond, it has a good heat storage possibility because of its huge thermal inertia.

This thesis has investigated both experimental and numerical analyses of a salt gradient solar pond. In the experimental analysis, performance evaluation of the solar pond was conducted, whereas in the numerical analyses, modeling in COMSOL was used to estimate the pond temperatures based on inputs of the experimental data and parametric studies including variations in weather conditions and pond dimensions.

According to the experimental analyses, the temperature of the lower convective zone is higher than both ambient temperature and upper convective zone temperature, since incoming solar radiation is mostly trapped on LCZ. Therefore, it proves that solar insolation is able to reach the bottom layer of the pond. Additionally, when the incoming solar radiation is high, higher LCZ temperature is maintained. For example, the highest LCZ temperature was observed when wind speed was considerably high, and the ambient air temperature was low. This is due to the increasing incoming solar insolation that reached the surface area of the pond. Hence, neither higher wind speeds nor lower ambient temperatures have a significant effect on the LCZ temperature. The main reason might be the high heat capacitance of the LCZ and thermal insulation around the solar pond.

Furthermore, UCZ temperature was mostly affected by wind speed due to its position. For instance, higher convective losses from UCZ to the outside were observed during the experimental analyses. Therefore, the relationship between temperature gradient

and heat transfer coefficient was investigated. Based on calculations, heat transfer rate was negative at some points, which proves that convective heat loss occurs from UCZ to the atmosphere. Because of the high convective losses, UCZ temperature was lower than expected. Hence, increasing convective heat transfer coefficient resulted in increasing heat transfer rate through the surrounding.

As a result, GHI had a more significant impact on controlling the temperature of the layers than ambient temperature and wind speed. It directly controlled the temperature trend of LCZ. Similarly, it also controlled the UCZ temperature but due to the presence of convective heat transfer and changes in ambient temperature; changes in UCZ temperature were not fully similar to the GHI variations. Hence, a compromise existed between the effect of GHI and ambient temperature of UCZ temperature.

In the experimental analyses, combined effect of weather conditions including incoming solar insolation, wind speed, and ambient temperature were exposed; thus, it was hard to evaluate their effects separately. Additionally, it was impossible to change the diameter or the layer thicknesses on the constructed solar pond in the experimentation. As a result, the numerical model in COMSOL was developed to investigate the effects of these parameters under the parametric studies.

In the first step of the numerical analyses, temperatures obtained from transient, numerical simulations using 10-minute and 2-hour intervals were compared with the experimental results for five arbitrarily chosen days. For the results with 10-minute interval, temperature gradient between the simulation and the experiments for each layer found as about 3ºC, which was in uncertainty range; thus, it validated the numerical modeling results with the experiments. Generally, temperatures found in COMSOL was either slightly higher or close to experimental data. Lower UCZ temperatures on the experimental results might be explained by heat loss through the outside of the solar pond. On the other hand, based on simulation results, UCZ temperatures were close to the ambient air temperatures since the model assumed that no evaporation and no salt diffusion occurred during the process.

Additionally, the simulation was run based on initial variables, and the program assumed that these variables did not change with time. This was the main reason for obtaining lower temperature differences between the layers for the results with 10-

minute interval since there was not a huge change on the layer temperatures during this short interval. However, high temperature differences were observed during the 2-hour intervals when it was compared to the experimental results. The main reason was that incoming solar insolation, wind speed and ambient temperature were not constant during 2 hours for experimental case, but in the numerical model, these parameters were constant.

Investigating the effects of climate conditions is the first part of the parametric analysis. It has been found that both UCZ and NCZ temperatures increased with increasing GHI, except for the LCZ temperature because incoming solar radiation cannot penetrate through the bottom layer of the pond. About 1.5ºC reduction in LCZ was observed for each defined GHI, which can be explained by the heat loss through the pond walls and ground. Moreover, it can be observed that wind speed does not have a profound effect on both NCZ and LCZ temperature. However, it affects UCZ temperature because of its position, the highest and the fastest variations are observed in this layer. Additionally, based on the results, ambient temperature has the highest effect on the layer temperatures, since the highest temperature variations in each layer, even if LCZ, are maintained during the variations in the ambient temperature.

Finally, effects on pond geometry on the layer temperatures was examined. Based on the analyses of pond geometry, it has been found that diameter does not affect the layer temperatures. Furthermore, based on the adjusted layer thickness, obtained temperature gradients for each zone were found close to each other; thus, it does not give a clear result. As a result, a more detailed simulation program is needed. In other words, to obtain more accurate results, it is better to use a more transient model, which can assume evaporation rate and diffusion of salt inside the SGSP. It is important to consider these assumptions since stability of a solar pond has been influenced by these factors including upward salt diffusion, salt type, heat flux, evaporation rate as well as the amount of wind.

For future work aspect, as mentioned above, it is required to investigate a transient model for a SGSP to obtain results that are more accurate. Besides, collecting long-period data can be used for better examination of the performance of the solar pond. Additionally, using transparent cover materials over the surface of the pond can be examined in detail because they can prevent evaporation and heat loss. As a result, the

amount of stored sustainable energy in the lower layer might increase, which can directly increase the overall efficiency of a SGSP.

REFERENCES

Akbarzadeh, A., Andrews, J., & Golding, P. (2009). Solar ponds. *Solar Energy Conversion and Photoenergy System-Volume I*, *8*, 242.

Amar, M. (2013). Energy consumption and economic growth: The case of African countries. *The Journal of Energy and Development*, *38*(1/2), 65-78.

Andrews, J., & Akbarzadeh, A. (2005). Enhancing the thermal efficiency of solar ponds by extracting heat from the gradient layer. *Solar Energy*, *78*(6), 704-716.

Angeli, C., & Leonardi, E. (2004). A one-dimensional numerical study of the salt diffusion in a salinity-gradient solar pond. *International journal of heat and mass transfer*, *47*(1), 1-10.

Angeli, C., Leonardi, E., & Maciocco, L. (2006). A computational study of salt diffusion and heat extraction in solar pond plants. *Solar Energy*, *80*(11), 1498-1508.

Bell, S. (1999). Measurement Good Practice Guide No. 11 (Issue 2), 41.

Beniwal, R. S., & Singh, R. (1987). Calculation of thermal efficiency of salt gradient solar ponds. *Heat Recovery Systems and CHP*, *7*(6), 497-516.

Bentley, J. P. (1984). Temperature sensor characteristics and measurement system design. *Journal of Physics E: Scientific Instruments*, *17*(6), 430.

Berkani et al, (2015). *Comparison of three solar ponds with different salts through bi-dimensional modeling.*

Bernad, F., Casas, S., Gibert, O., Akbarzadeh, A., Cortina, J. L., & Valderrama, C. (2013). Salinity gradient solar pond: validation and simulation model. *Solar energy*, *98*, 366-374.

Bergman, T. L., & Incropera, F. P. (2011). *Fundamentals of heat and mass transfer*. John Wiley & Sons.

Boudhiaf, R., Moussa, A. B., & Baccar, M. (2012). A two-dimensional numerical study of hydrodynamic, heat and mass transfer and stability in a salt gradient solar pond. *Energies*, *5*(10), 3986-4007.

Cox, R. A., & Smith, N. D. (1959, August). The specific heat of sea water. In *Proceedings of the Royal Society of London A: Mathematical, Physical and Engineering Sciences* (Vol. 252, No. 1268, pp. 51-62). The Royal Society.

Chinn et al, (2003). *The Design, Construction, Operation & Maintenance of an Experimental Magnesium Chloride Solar Pond.*

Dell, R. M., & Rand, D. A. J. (2001). Energy storage—a key technology for global energy sustainability. *Journal of Power Sources*, *100*(1), 2-17.

Dincer, I. (2000). Renewable energy and sustainable development: a crucial review. *Renewable and Sustainable Energy Reviews*, *4*(2), 157-175.

Dincer, I., & Rosen, M. A. (2012). *Exergy: Energy, environment and sustainable development*. Newnes.

Enshayan, K. (1989). *Measurement of solar radiation transmission in solar ponds* (Doctoral dissertation, The Ohio State University).

Garmana, M. A., & Muntasserb, M. A. (2008). Sizing and thermal study of salinity gradient solar ponds connecting with the MED desalination unit. *Desalination, 222* (1-3), 689-695.

Goutham, K., & Krishna, C. S. (2013). Solar pond technology. *Int. J. Eng. Res. Gen. Sci*, *1*(2), 12-22.

Jubran, B. A., Al-Abdali, H., Al-Hiddabi, S., Al-Hinai, H., & Zurigat, Y. (2004). Numerical modelling of convective layers in solar ponds. *Solar energy*, *77*(3), 339-345.

Kaygusuz, K. and Toklu, E. (2012). Energy issues and sustainable development in Turkey, Journal of Engineering Research and Applied Science, vol. 1, no. 1, pp. 1-25, 2012.

Kumar, M., Mishra, A., Kumar, S., Yadav, A. K., & Pal, V. (2016). *Solar Pond.* IJCA Proceedings on National Conference on Role of Engineers in National Building NCRENB 2016(2):20-24.

Kurt, H., Ozkaymak, M., & Binark, A. K. (2006). Experimental and numerical analysis of sodium-carbonate salt gradient solar-pond performance under simulated solar-radiation. *Applied energy*, *83*(4), 324-342.

Leblanc, J., Akbarzadeh, A., Andrews, J., Lu, H., & Golding, P. (2011). Heat extraction methods from salinity-gradient solar ponds and introduction of a novel system of heat extraction for improved efficiency. *Solar Energy*, *85*(12), 3103-3142.

Monjezi, A. A., & Campbell, A. N. (2016). A comprehensive transient model for the prediction of the temperature distribution in a solar pond under Mediterranean conditions. *Solar Energy*, *135*, 297-307.

Mostafa H. Sharqawy, John H. Lienhard V, and Syed M. Zubair, "Thermophysical properties of seawater: A review of existing correlations and data," Desalination and Water Treatment, Vol. 16, pp.354-380, April 2010.

Multiphysics, COMSOL. Introduction to COMSOL Multiphysics®. *COMSOL Multiphysics, Burlington, MA, accessed Feb*, 1998, 9: 2018.

Multiphysics, COMSOL (2014). Heat Transfer Module User's Guide. *Documentation within Software Package, Ver, 4*.

Nalan, B. C., & Arzu, Ş. Ş. (2011). Thermal efficiency for each zone of a solar pond. *Chinese Physics Letters, 28*(10), 108902.

Oberhofer, A., & Meisen, P. (2012). Energy Storage Technologies & Their Role in Renewable Integration. *Global Energy Network Institute*

Patel, A. P. R. (2015). Designing of Portable Solar Pond for Improved Efficiency.

Sathish, D. (2015). Effective study on solar pond and its various performances.

Sharqawy, M. H., Lienhard, J. H., & Zubair, S. M. (2010). Thermophysical properties of seawater: a review of existing correlations and data. *Desalination and water Treatment*, *16*(1-3), 354-380.

Siegel, R. (2001). *Thermal radiation heat transfer* (Vol. 1). CRC press.

Singh, R., Tundee, S., & Akbarzadeh, A. (2011). Electric power generation from solar pond using combined thermosyphon and thermoelectric modules. *Solar Energy*, *85*(2), 371-378.

Srinivasan, J. (1993). Solar pond technology. *Sadhana*, *18*(1), 39-55.

Suárez, F., Childress, A. E., & Tyler, S. W. (2010). *Temperature evolution of an experimental salt-gradient solar pond. Journal of Water and Climate Change, 1(4), 246-250.*

Sukhatme, K., & Sukhatme, S. P. (1996). *Solar energy: principles of thermal collection and storage*. Tata McGraw-Hill Education.

Tabor, H., & Matz, R. (1965). A status report on a solar pond project. *Solar Energy*, *9*(4), 177-182.

Taylan O., Ahmed H., Guven P. (2017), "Dissociation of CO_2 Using Salt Gradient Solar Pond", 2nd International Mediterranean Science and Engineering Congress (IMSEC 2017), 25-27 October 2017, Adana, Turkey.

Tester, J. W. (2005). *Sustainable energy: choosing among options*. MIT press.

Torkmahalleh, M., Askari, M., Gorjinezhad, S., Eroğlu, D., Obaidullah, M., Habib, A. R., … Ahmadi, G. (2017). Key factors impacting performance of a salinity gradient solar pond exposed to Mediterranean climate. *Solar Energy, 142*, 321–329.

Tundee, S., Terdtoon, P., Sakulchangsatjatai, P., Singh, R., & Akbarzadeh, A. (2010). Heat extraction from salinity-gradient solar ponds using heat pipe heat exchangers. *Solar Energy*, *84*(9), 1706-1716.

Twidell, J., & Weir, T. (2015). Renewable energy resources. Routledge.

Valderrama, C., Cortina, J. L., & Akbarzadeh, A. (2016). Solar Ponds. In *Storing Energy* (pp. 273-289).